AWARD NUMBER: W81XWH-13-1-0073

TITLE: 7T Magnetization Transfer and Chemical Exchange Saturation Transfer MRI of Cortical Gray Matter: Can We Detect Neurochemical and Macromolecular Abnormalities?

PRINCIPAL INVESTIGATOR: Seth A. Smith

CONTRACTING ORGANIZATION: Vanderbilt University
Nashville, TN 37240

REPORT DATE: October 2015

TYPE OF REPORT: Annual

PREPARED FOR: U.S. Army Medical Research and Materiel Command
Fort Detrick, Maryland 21702-5012

REPORT DOCUMENTATION PAGE

Form Approved
OMB No. 0704-0188

1. REPORT DATE	2. REPORT TYPE	3. DATES COVERED
October 2015	Annual	30 Sep 2014 - 29 Sep 2015

4. TITLE AND SUBTITLE

7T Magnetization Transfer and Chemical Exchange Saturation Transfer MRI of Cortical Gray Matter: Can We Detect Neuro-chemical and Macromolecular Abnormalities?

5a. CONTRACT NUMBER

5b. GRANT NUMBER
W81XWH-13-1-0073

5c. PROGRAM ELEMENT NUMBER

6. AUTHOR(S)
Seth Smith

E-Mail: seth.smith@vanderbilt.edu

5d. PROJECT NUMBER

5e. TASK NUMBER

5f. WORK UNIT NUMBER

7. PERFORMING ORGANIZATION NAME(S) AND ADDRESS(ES)

The Vanderbilt University
Nashville, TN 37240-0001

8. PERFORMING ORGANIZATION REPORT NUMBER

9. SPONSORING / MONITORING AGENCY NAME(S) AND ADDRESS(ES)

U.S. Army Medical Research and Materiel Command
Fort Detrick, Maryland 21702-5012

10. SPONSOR/MONITOR'S ACRONYM(S)

11. SPONSOR/MONITOR'S REPORT NUMBER(S)

12. DISTRIBUTION / AVAILABILITY STATEMENT

Approved for Public Release; Distribution Unlimited

13. SUPPLEMENTARY NOTES

14. ABSTRACT

We present the second annual report for this project. We have developed and deployed a quantitative MRI set of MRI scans at 7T in healthy volunteers and patients with MS, developed an analysis pipeline and QA for the quantification of macromolecular and metabolic indices reflective of demyelination and neurotransmitter/protein accumulation. All quantitative acquisitions have been evaluated for reproducibility. Behavioral testing shows significant differences between MS and healthy volunteers, along with fMRI, and CEST acquisitions. Analysis hurdles were noted in the qMT, which we discuss here. Recruitment continues in the MS cohort (all healthy subjects have been recruited) during the EWOF. Correlation analysis have been examined, and a translation to lower field strength has generated many further outcomes.

15. SUBJECT TERMS

16. SECURITY CLASSIFICATION OF:			17. LIMITATION OF ABSTRACT	18. NUMBER OF PAGES	19a. NAME OF RESPONSIBLE PERSON
a. REPORT	b. ABSTRACT	c. THIS PAGE			USAMRMC
U	U	U	UU	37	19b. TELEPHONE NUMBER *(include area code)*

Table of Contents

INTRODUCTION:
We recognize that many patients with Multiple Sclerosis (MS) suffer from cognitive impairment at some point in their disease course. However, characterization cognitive change in patients with MS has been difficult to pinpoint, and is hampered by poor quantitative markers. We have two hypotheses: 1) conventional imaging is insensitive to gray matter (GM) changes known to exist in patients with MS, and 2) ultra-high MRI field strengths (7T) would allow an opportunity to study the myelination and metabolic changes of the cortical GM in patients with MS and known cognitive impairment. The purpose of this proposal is to develop and implement a targeted quantitative magnetization transfer (qMT) and chemical exchange saturation transfer (CEST) MRI imaging paradigm at 7T to detect and quantify the level of myelin loss (qMT), protein/peptide changes (amide proton transfer CEST), neurotransmitter deficiencies (GluCEST) in the GM of patients with MS, and to relate these findings to neuropsychiatric evaluation outside the MRI scanner. The scope is to: 1) develop novel, high-resolution, high field, quantitative MRI methods sensitive to myelination and neurochemicals for implementation in the cortical GM of human populations, 2) deploy these methods in patients with MS, 3) relate these findings to measures of cognitive impairment, and 4) develop a lower MRI field strength alternative for direct patient impact.

KEYWORDS:
- Magnetic Resonance Imaging (MRI)
- 7 Tesla (7T)
- Chemical Exchange Saturation Transfer (CEST)
- Magnetization Transfer (MT)
- Brain
- Cortical Gray Matter (cGM)
- Multiple Sclerosis (MS)
- Functional MRI (fMRI)
- Pool Size Ratio (PSR)
- Amide Proton Transfer (APT)
- Glutamate (Glu)
- Cognitive Impairment

OVERALL PROJECT SUMMARY

Task 1. *IRB Preparation and Human Subjects Approvals.*

Status: Completed

Task 2*. Develop, optimize and implement advanced, quantitative Magnetization Transfer (MT) and Chemical Exchange Saturation Transfer (CEST) in phantoms and evaluate minimum achievable resolution and the associated reliability of derived indices*

Status: Completed

Y1 Summary of Protocol implemented in healthy controls (Task 3) and patients with MS (Task 5). No modifications were performed in year 2.
- Constant RF APT CEST – 9:10
- Constant RF GluCEST – 11:36
- SIR qMT – 10:11
- Bloch-Siegert B1 mapping – 1:42
- Dual-echo B0 mapping – :04

- T1w MPRAGE Anatomical – 2:12
- fMRI Resting State – 8:34
- fMRI N-Back task – 8:30
- fMRI Trailmaking task – 4:14

The current scan time for all scans is approximately 1 hour.

Task 3 – *Implement current best practice for MT and CEST in healthy volunteers and evaluate reliability*

The objective of this task was to implement a best-practice MT, CEST, task-based fMRI, and resting-state fMRI (rs-fMRI) acquisition scheme in healthy controls and develop a pipeline for robust analysis, quality assurance, and interpretation.

Status: Completed

Summary of Results/Progress and Accomplishments
The above Y1 Summary Protocol has been implemented in 55 healthy volunteers (39 females, mean age = 31 ± 8years) at the close of year 2. Of those 55, we have obtained reliability/reproducibility data in 10 volunteers.

One of the most important developments in year 2 was to construct an automatic data storage, analysis, and quality assessment pipeline. The importance of this cannot be underestimated as immediately after the data is acquired, the data is shuttled off to our internal PACS system, and "spiders" (Python-based programming scripts based off of Matlab processing modules) reside in the database to capture the data, pre-process all of the data, and generate reports similar to those shown in **Appendix 1** (for fMRI). These allow us to, at a glance, determine the fidelity of the acquisition, characterize any gross motion, and pre-process the data for further analysis. This has dramatically reduced our time from scan to analysis in this year. Similar pipelines have been written for CEST and qMT analysis, though their incorporation into "spiders" is ongoing as we are actively investigating alternative analysis strategies throughout this year.

Task 4 – *Analyze the derived indices in healthy volunteers and evaluate reproducibility (1 month)*

The objective of this task was to 1) develop an analysis pipeline for constructing maps and deriving indices reflective of GM and WM from the quantitative MRI acquisitions prepared in Task 3

Status: Completed

Summary of Results/Progress and Accomplishments
Many of the results from Task 4 have been shown in Y1 progress report(s) and summarized in quarterly progress reports through Y2. Here we present a summary of each of the acquisitions and their derived indices.

APT CEST analysis and results
For APT and GluCEST analysis, we performed motion correction (within scan), co-registration (between scans) and WM/GM segmentation. All pre-processing of motion correction, coregitration, and segmentation was performed in FSL (FMRIB, Oxford, UK) and written into a Matlab wrapper for automated pre-processing. In summary, motion correction was performed using a 12-degree of freedom linear affine procedure (FSL FLIRT), co-registration (CEST acquisitions were coregistered to the MPRAGE) was performed using FNIRT (non-linear registration in FSL), and segmentation in to 3 classes (WM, GM, and CSF/Lesion) was performed in FAST (FSL). The WM/GM segmented classes were then applied to the derived APT and GluCEST maps. A similar procedure for qMT is outlined below.

After motion correction and coregistration, we have constructed the APT CEST maps in the following manner. First, the CEST spectrum for each voxel is normalized, corrected for B1 drift and fit to a single-lorentizian (11) and the minimum spectral intensity is shifted to an offset ($\Delta\omega$) = 0 for B0 correction. After this correction, we calculate the CEST asymmetry ($CEST_{asym}$) between $\pm\Delta\omega$ signals at various offset frequencies ($\Delta\omega$). To assess reproducibility we created a single CEST z-spectrum for each participant and a calculated histograms for the GM $CEST_{asym}$ at $\Delta\omega$ = 2, 3, and 3.5ppm. **Figure 1** shows the anatomical MPRAGE, GM segmentation results, and CESTasym maps for visit 1 and visit 2. Additionally, we overlay histograms for GM CESTasym for each visit for each of the offsets listed above. Statistically, there are not differences in the spread, or median of the histograms for GM. Additionally, we compared APT-CEST using Bland-Altman analyses and at the α = 0.05 level, no differences were noted.

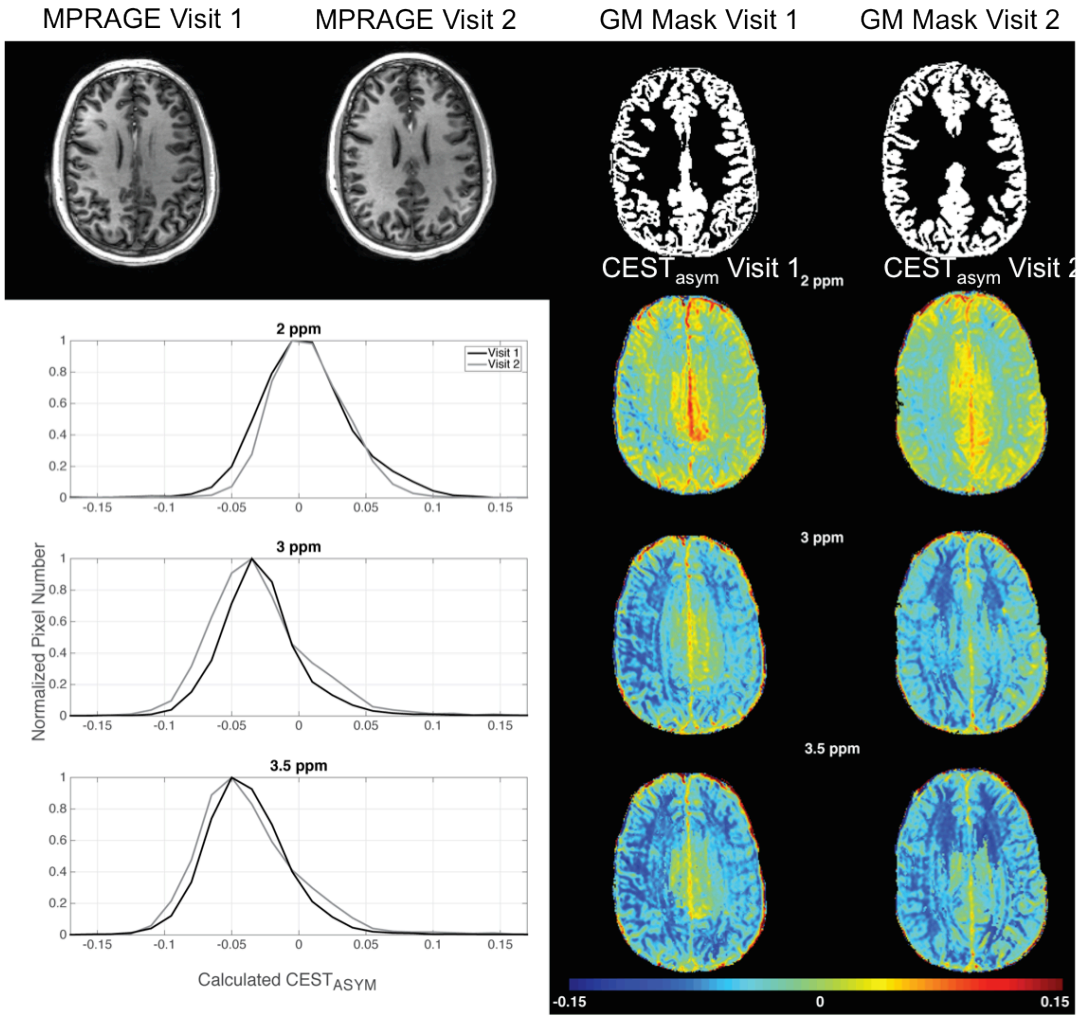

Figure 1: Comparison of anatomical, segmentation, $CEST_{asym}$ maps for Dw = 2, 3, and 3.5 ppm. Additionally $CEST_{asym}$ histograms in GM of healthy volunteers show high degree of overlap indicating no significant differences between scanning sessions.

Glutamate CEST (GluCEST) analysis and results

GluCEST analysis proceeded as presented in (8,9). In a similar fashion, we derived the GluCEST asymmetry at 2, 3, and 3.5ppm (though we expect the 3.0ppm offset to be of interest due to its sensitivity to Glutamate). **Figure 2 (top)** shows overall GluCEST z-spectra in healthy volunteers (**blue**) and MS patients (**red**) with the solid line indicating the median of GM GluCEST values and the shaded region the standard deviation over all participants. Bland-Altman analysis, **Figure 2 (bottom)**, is shown for the healthy volunteers indicating excellent reproducibility. The coefficient of reproducibility was 0.053 indicating that any absolute difference greater than 0.053 would yield a significant difference at the α = 0.05 level. Further discussion of the differences between the cohorts is given in Task 5.

Quantitative Magnetization Transfer (qMT) analysis and results

In all participants, we obtained high-resolution selective inversion recovery (SIR) qMT and analyzed the data according to (10) to generate the pool size ratio (PSR), exchange rate (kmf), and longitudinal relaxation rate (R1f). In short, an inversion recovery MRI sequence was performed using a modified inversion pulse that is

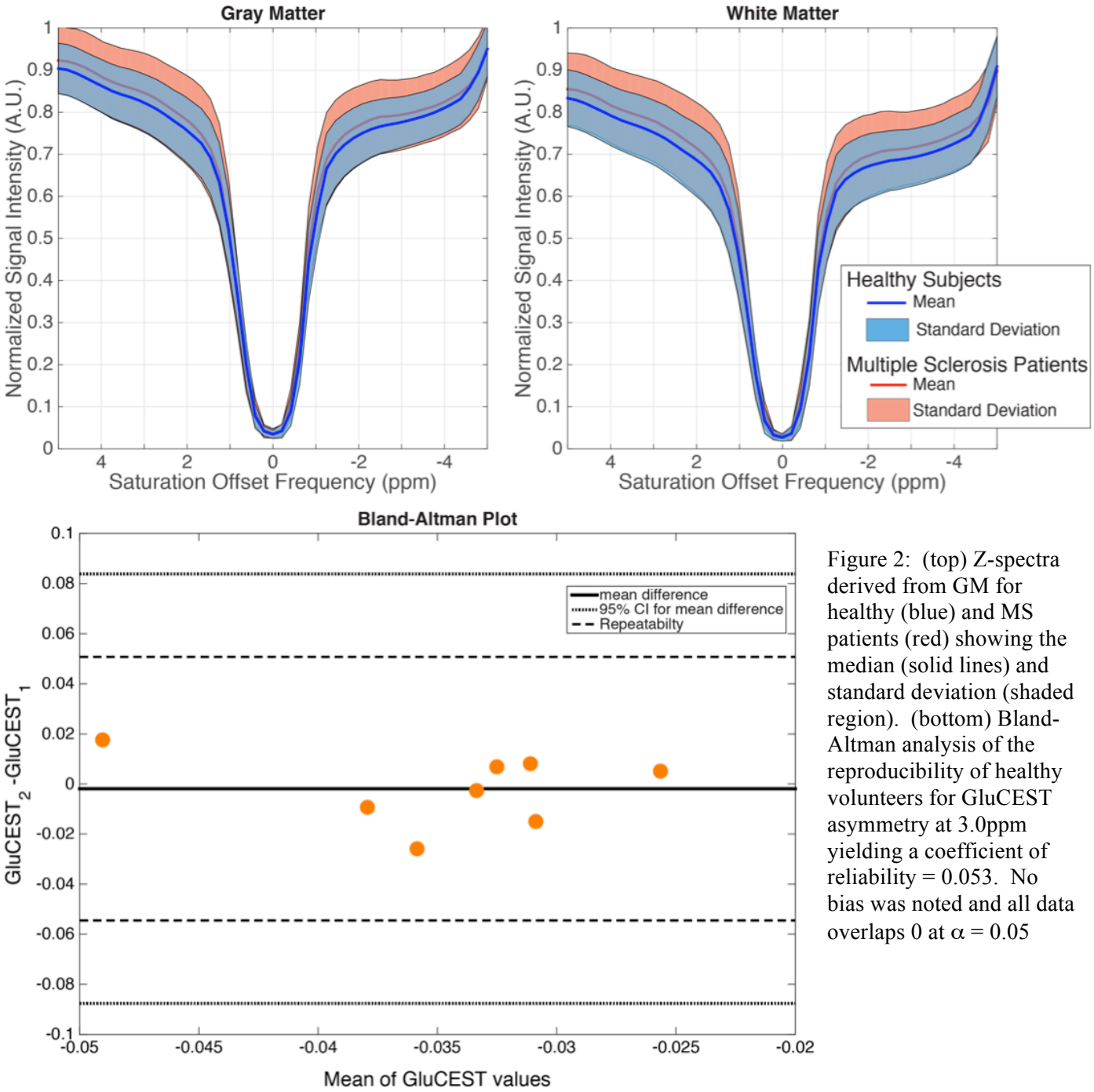

Figure 2: (top) Z-spectra derived from GM for healthy (blue) and MS patients (red) showing the median (solid lines) and standard deviation (shaded region). (bottom) Bland-Altman analysis of the reproducibility of healthy volunteers for GluCEST asymmetry at 3.0ppm yielding a coefficient of reliability = 0.053. No bias was noted and all data overlaps 0 at $\alpha = 0.05$

relatively insensitive to B1 and B0 inhomogeneities. The inversion times were selected to sample the bi-exponential recovery known to exist when magnetization transfer is present. For every voxel, the SIR signal equation was fit to the recovery curve and the exchange rate (kmf), pool size ratio (PSR) and longitudinal relaxation time (R1f) was fit. Once maps of each index were calculated, we analyzed the data further as follows.

To mitigate B1 inhomogeneity further (which can be problematic for segmentation), we divided the qMT-weighted images obtained at the 10^{th} and 14^{th} inversion time to create an image with similar image quality as the MPRAGE. From that, WM, GM, and CSF/Lesion were segmented used the FAST segmentation algorithm

supplied in FSL. We noticed that in some cases, some voxels were incorrectly classified as white or gray matter (a larger challenge in the MS patients and described below in Task 5) and thus, a semi-automated method was employed to remove spuriously classified voxels. Additionally, kmf at tissue boundaries often times is poorly fit, thus, we performed a secondary outlier rejection on data that was greater than 2 STD of the mean and set that data to the maximum (or minimum) value with in the tissue. After segmentation, the WM, and GM masks were transferred to the PSR, kmf, and R1f data and histograms for all white and gray matter were created. We chose to analyze the histograms in 3 ways: 1) the location of the peak height (effectively the Mode, P0), 2) the spread of the histogram (full-width at half maximum, FWHM), and 3) the median. The importance of this cannot be under appreciated as it allows us to look at the spread of the data (in MS, we expect that GM may have a greater spread, but a median that is similar to the healthy volunteers) in addition to the peak height (irrespective of histogram tails). Detailed evaluation of this in the MS patients is given in Task 5.

From these analyses, we focus primarily on the PSR, which is an indicator of myelin for Task 5. Using each of the indices characterizing the histogram, we found the following PSR values in healthy volunteers (mean ± STD):
P0 WM = 15.1 ± 3.0, P0 GM = 9.8 ± 4.1
FWHM WM = 7.6 ± 2.7, FWHM GM = 12.6 ± 5.8
Median WM = 18.1 ± 2.8, Median GM = 13.3 ± 2.2

rs-fMRI analysis and results

rs-fMRI analysis proceeded as shown in the poster (**Appendix 2**). In summary, preprocessing steps included: 1) motion correction (all dynamics to the first dynamic), 2) slice timing correction, 3) segmentation of MPRAGE acquisition into WM, GM, and CSF classes, 4) coregistration of rs-fMRI maps into standard space, 5) normalization of GM masks to the MNI GM template, and 6) a smoothing of functional voxels using a 6mm FWHM kernel. All data were processed in SPM12 and the processing pipeline is shown in **Figure 3**.

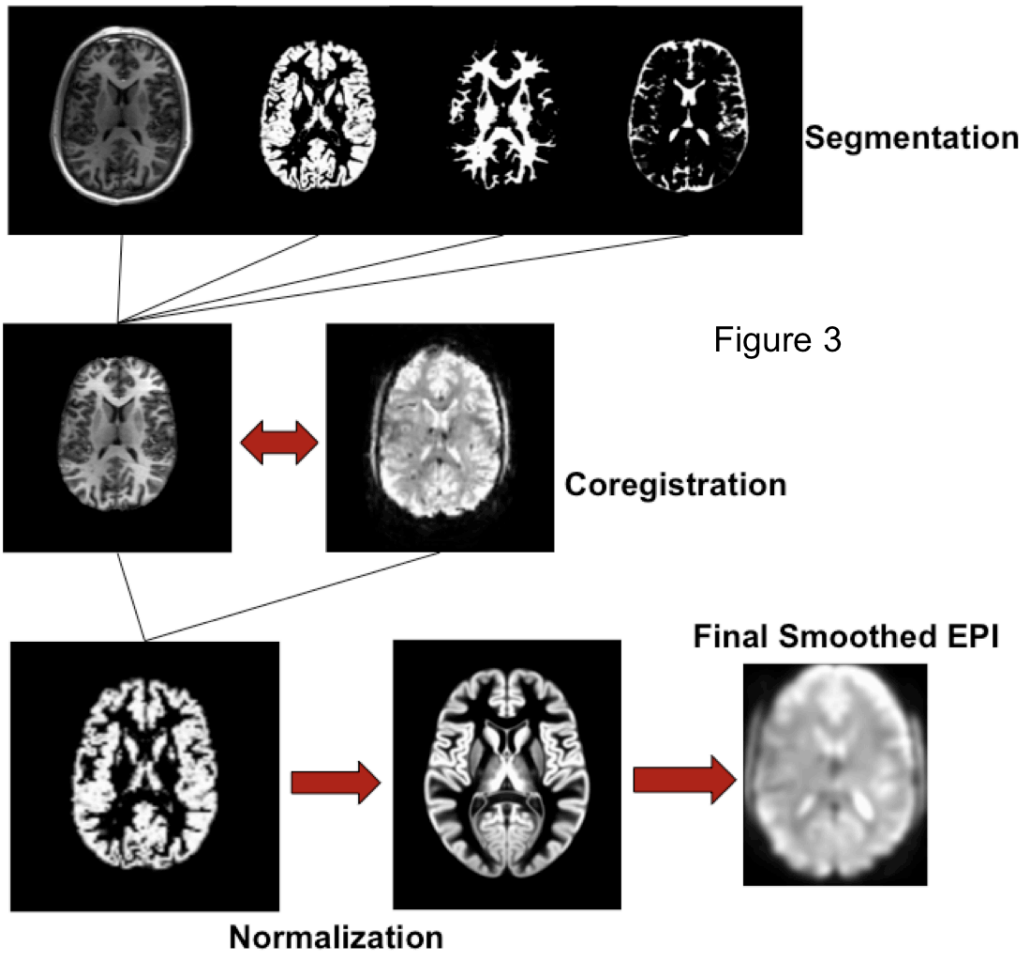

Figure 3

Task-based fMRI analysis and results

During this year, we have focused on the resting-state analysis and results, though we have built similar pipelines for analysis for the task-based fMRI methods. We are currently (during the EWOF) analyzing the task-based results for comparison with neuropsychiatric evaluation (Task 6).

Task 5 – Implementation in Patients with MS and concomitant cognitive impairment
The objective of this task is to deploy, and analyze the MRI acquisitions in patients with MS.

Status: Active, not yet complete

We have implemented the MRI paradigm in 37 patients with MS (28 Female, mean age = 38 ± 5 years) and have been approved for an EWOF to obtain data in the remaining 13 volunteers. We expect no delays in obtaining data in the final 13 patients.

In all MS patients, the analysis proceeds with the same methodology as presented for Task 4 (healthy volunteers), and any exceptions are noted in the text below.

APT CEST results

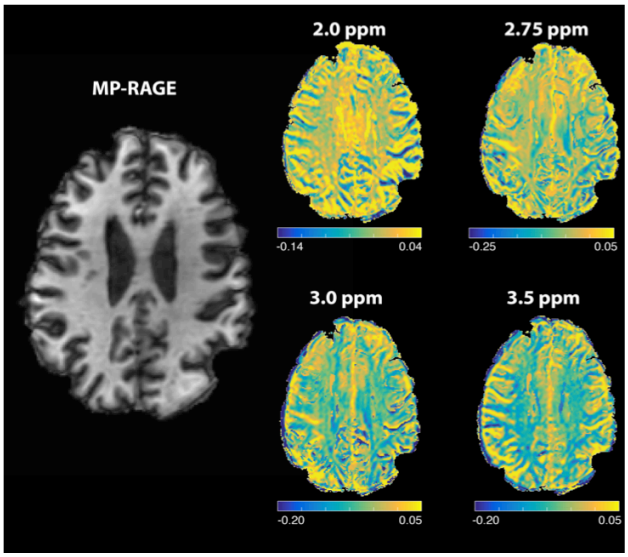

Figure 4: 42y.o. female MS patient with CESTasym maps derived from the APT CEST protocol.

APT CEST data were obtained with excellent image quality in patients with MS. Figures **4 and 5** show two examples of maps at Δω = 2, 2.5, 3, and 3.5ppm along with the corresponding MPRAGE anatomical image. **Figure 4** compares the APT CEST ($CEST_{asym}$) maps in a 42 year old female MS patient. Note in this particular patient the amount of atrophy is larger than is seen in **Figure 5** (38 year old female MS patient) and the noted GM/WM contrast derived from Δω = 3.5ppm is slightly lower than is seen from the patient in **Figure 5**. These two figures highlight the differences among patients as seen with CEST imaging, which we are characterizing during the EWOF.

Glutamate CEST (GluCEST) results

GluCEST data were obtained and processed according to the methods outlined above. **Figure 2** shows the average GluCEST z-spectra in the MS patients compared to the healthy controls. Compared to the healthy controls, the MS patients showed an upward trend in the CEST z-spectra for all positive offset frequencies and an elevated GluCEST signal at 3.0ppm. We then calculated the histograms for 2.75, 3, and 3.5ppm for healthy volunteers (blue) and all patients with MS (red) and show those results in **Figure 6**. All histograms were taken from segmented GM. For the healthy volunteers, the GM GluCEST histograms are largely unimodal and centered at 0 (indicating little to no GluCEST asymmetry). However, when comparing to the MS patients, two things are noted. First, the distributions for the MS patients at Δω = 2.75, 3, and 3.5ppm show a non-unimodal (bimodal) distribution and secondly, there is a slight upward bias in the distributions, especially for Δω = 3.0ppm. We take this to mean that there is some GM with lower GluCEST asymmetry than healthy volunteers, and some GM with increased GluCEST asymmetry. We

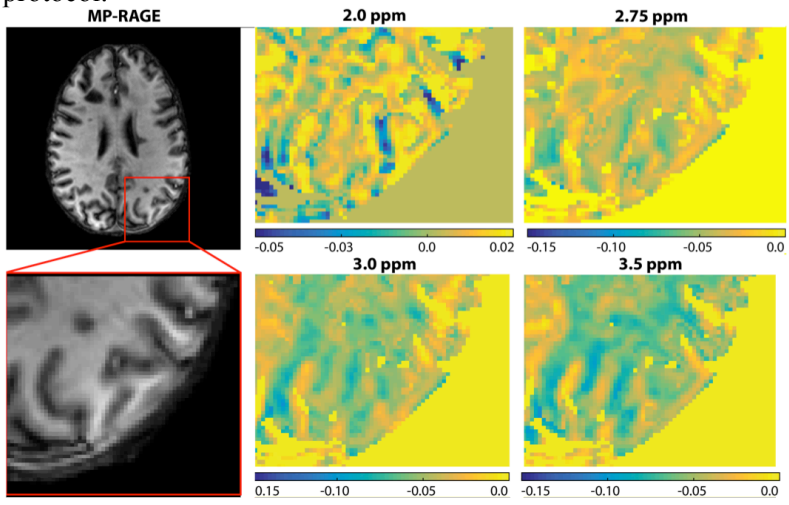

Figure 5: 38y.o. female MS patient with CESTasym maps derived from the APT CEST protocol.

will connect these GM tissues with those identified by the resting state fMRI to determine of the increase (and decrease) in functional connectivity is at all related to the locations of increased (and decreased) GluCEST asymmetry signals.

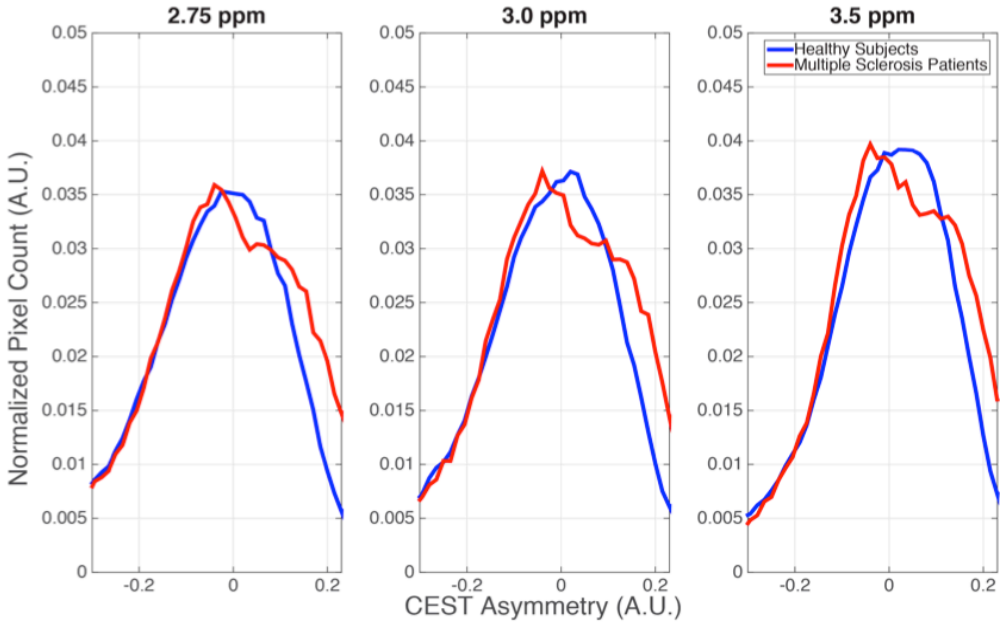

Figure 6: GluCEST asym histograms for GM at Δω = 2.75, 3.0, and 3.5ppm. Note the non-unimodal distributions in the MS cohort (red) relative to the healthy (blue)

Quantitative Magnetization Transfer (qMT) analysis and results

qMT-derived PSR, kmf, and R1f were generated as given in Task 4, with one small change for the patients with MS. When performing FAST segmentation in the MS patients (with only 3 segmentation classes) sometimes, lesions will be classified as white matter, gray matter, or CSF. In the cases where lesions were classified as GM, we wanted to mitigate the impact that this could have on looking at the GM across patient cohorts. Thus, we performed a secondary analysis to remove lesions from any WM, GM, and CSF class and discarded those voxels. The impact is two fold: 1) when removing lesions from the white matter, the white matter PSR increases such that it becomes more similar to healthy white matter (thus statistical comparisons can be minimized), but 2) it increases the confidence that we have that the PSR is a reflection of myelination of otherwise normal appearing white and gray matter. We believe that lesions are largely un-noticed in GM, thus we want to compare the GM in the absence of lesion contamination.

PSR

P0				**FWHM**			
WM		**GM**		**WM**		**GM**	
CTL	*MS*	*CTL*	*MS*	CTL	MS	CTL	MS
15.1 ± 3.0	12.1 ± 4.8	9.8 ± 4.1	8.5 ± 4.0	7.6 ± 2.7	10.5 ± 3.7	12.6 ± 5.8	15.02 ± 6.2
p-value = 0.015		*p-value = 0.11*		**p-value = 0.002**		**p-value = 0.03**	

Median			
WM		**GM**	
CTL	*MS*	*CTL*	*MS*
18.1 ± 2.8	18.2 ± 4.1	13.3 ± 2.2	12.3 ± 3.2
p-value = 0.45		*p-value = 0.12*	

To that end, we have performed simple 1 tailed student's t-test between the 3 characterizations of the WM and GM histograms across cohorts: P0, FWHM, and median. We chose a 1-sample t-test because the PSR should decrease in MS (we do not expect hypermyelination), and we chose to employ unequal variance for all tests. A summary of the PSR findings is given in **Table 1**. The p-values given in red reflect statistical differences between the two cohorts. Some important findings are noted. First, there is a statistical downward difference in the MS WM P0 compared to the healthy volunteer indicating that qMT-PSR is showing loss of myelination in the normal appearing white matter. Secondly, the FWHM is greater in the MS cohort for both WM and GM indicating the greater variance in the histograms (i.e. there is a larger data spread in MS). Interestingly, the median value is not statistically different between the two cohorts. We hypothesize that this is due to 1) the variance in the data is larger for MS relative to the healthy cohort, while the actual P0 is about the same, and 2) histogram analysis loses spatial information, thus there is averaging among damaged and non-damaged WM and GM. We will look only at fMRI-localized zones of functional differences for further analysis during the EWOF.

rs-fMRI analysis and results

In a small cohort, we show the results of the rs-fMRI in patients compared to healthy volunteers in **Appendix 2**. A typical, and detailed analysis in a small cohort of patients for two particular networks is summarized in **Appendix 3**.

Task-based fMRI

We have nothing to report at the close of this annual report, but pre-processing, and detailed analysis is underway during the EWOF.

Task 6 – Cross-sectional analysis of derived indices between patients with MS and healthy volunteers and correlation with clinical measures of cognitive impairment derived from the Minimal Assessment of Cognitive Function in MS (MACFIMS)

The objective of this task is to compare quantitative MRI indices across cohorts, implement neuropsychiatric evaluations in both healthy and MS patient cohorts, and derive correlations with quantitative MR indices.

Status: Active, not yet complete

Neuropsychiatric Assessment Battery (Outside MRI Scanner)

We have obtained neuropsychiatric evaluations in healthy volunteers in addition to patients with MS. Therefore; we have obtained neuropsychiatric data using the paradigm below in 55 healthy volunteers (10 repeats) and 37 MS patients.

Summary of Tasks - Outside the scanner and BEFORE coming to Vanderbilt

Questionnaire and survey already developed in REDCap to be completed at home and in a calm environment. These surveys will collect data related to baseline mood, anxiety, and cognitive profile.

Summary of Tasks - Outside the scanner at Vanderbilt (< 1 hour total)

- Short measure of day-of mood/anxiety
- N-back test (2-back or 3-back): measures working memory
- PASAT: measures working memory
- Trail making test (both A and B): measures planning/executive function
- "Black Box" (choice reaction time, critical flicker fusion; pre-scan and post-scan): measures processing speed/reaction time
- *Buschke selective reminding test (8 trials): measures include encoding and long-term memory

- Digit Symbol Substitution Test/DDST: measures visual memory
- Posner cueing task: measures attentional shift

For this task, we have begun to analyze the data in two ways: 1) examining the neuropsychiatric tests between MS and healthy volunteers, and 2) drawing correlations between aspects of the neuropsychiatric tests and quantitative tests. **Table 2** shows a summary of the statistically different neuropsychiatric evaluations between healthy and MS patients.

Summary	MS vs. HC	p-value
SDMT		
	Completed Items	p < 0.0001
Revised BVMT-R		
	Total Recall	p = 0.0001
	Delayed Recall	p = 0.013
Buschke Selective Reminding		
	Total Recall	p = 0.002
	Consistency	p = 0.0006
	Recall Failure	p = 0.007
MMSE		
	Total Score	p = 0.006
PASAT		
	Raw Score	p = 0.0003
Trail Making Task		
	Part A (#)	P = 0.01
	Part B (#,Letters)	p = 0.001
Single/Choice Reaction Time		
	SRT	p < 0.0001
	CRT	p < 0.0001

Figure 7 shows two comparisons between GluCEST derived indices for GM at $\Delta\omega = 3.0$ppm and visuospatial memory test (**Figure 7, left**) and the global deterioration scale (**Figure 7, right**) indicating associations ($p = 0.01$ and $p = 0.06$). While this comparison serves as an anecdote for the comparisions we are performing, it should be noted that during the EWOF, there will be a more focused analysis, in that the analyses performed here, looks at the entire GM for correlation, and we would ideally, look at the segments that have been identified by fMRI to be abnormal in the MS cohort.

Task 7 – Translation to lower, more clinically relevant field strengths for greater impact
Status: Complete

During Y2, we have successfully translated the CEST and MT acquisitions to 3T for further clinical impact. To that end, we have not only successfully implemented novel CEST and MT acquisitions in the spinal cord and optic nerve, but also have disseminated these methods to collaborators outside of Vanderbilt for application to patients with brain tumors (see publications below). No further work on this task will be performed during the EWOF.

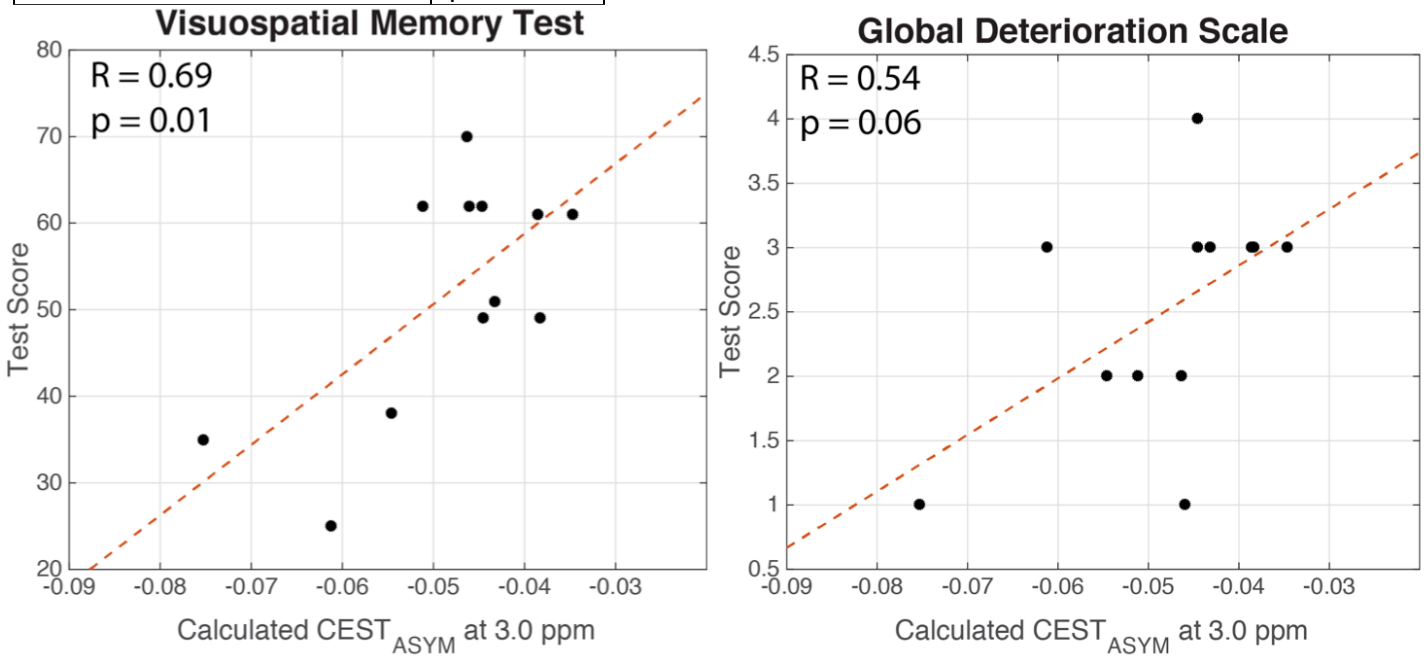

Figure 7: Two correlations between a small cohort (13 MS patients) comparing the association between GluCEST at 3.0ppm for GM and the Visuospatial Memory Test and Global Deterioration Scale

KEY RESEARCH ACCOMPLISHMENTS:

1. Developed an automatic processing pipeline and QA procedure for fMRI, qMT, and CEST acquisitions
2. Developed a combined automatic and semi-automatic segmentation algorithm to identify GM, WM, CSF and lesions in patients and healthy volunteers.
3. Completed Tasks 1-4, 7, with 37 (out of 50) MS patients completing the final evaluation methodology.
4. Identified networks in MS that are increased and decreased using resting-state fMRI
5. Developed a lower field (3T) alternative to MT, and CEST with applications to other anatomies and patient populations ongoing.
6. Developed a rich database of neuropsychiatric evaluation assessments in patients with MS and demonstrated the existence of differences compared to healthy volunteers.
7. Developed a complete qMT, CEST (APT and Glutamate), task-based fMRI, and resting-state fMRI battery for 7T evaluation of MS patients.

CONCLUSION:

We have concluded the second year of this project and have many significant contributions to report. We have been able to develop automatic analysis pipelines for a routine 7T exam card that allows for collection of data that reports on macromolecular content (qMT), protein/peptide concentration (APT CEST), neurochemical composition (GluCEST), resting-state functional connectivity (rs-fMRI), and task-based fMRI. Additionally, we have prepared an exhaustive selection of neuropsychiatric evaluations to be performed prior to MRI scanning. We completed a significant fraction of the tasks (tasks 1-6) with further data analysis, correlation studies, and associations between measurements to be performed during the EWOF. To this end, we have scanned 55 healthy volunteers (with 10 healthy volunteers participating in a repeat MRI examination), and 37 patients with MS. We will continue to recruit the final 13 patients during the EWOF. Importantly, Task 7 has been a success in that we have been able to develop, deploy, and disseminate at 3T alternative to qMT and CEST that has been used in multiple countries and patient populations. We are enthusiastic with the results, and look forward to wrapping up publications and analyses during the EWOF.

PUBLICATIONS, ABSTRACTS, AND PRESENTATIONS:

1. **Lay Press**: Interview with leading South Korean Media outlet (Chosun Biz) regarding CEST in clinical populations: http://biz.chosun.com/site/data/html_dir/2015/03/29/2015032901804.html
2. **Peer-Reviewed Scientific Journals**: Nothing to report
3. **Invited Articles**: Nothing to report
4. **Presentations**:

   Dula AN. OctoberCEST. 10/9/2015 VUIIS Friday Seminar

   Smith SA. Chemical Exchange Saturation Transfer (CEST): Basics, controversies, and clinical impact. 3rd Annual International Congress on MRI and 20th Annual KSMRM, Seoul South Korea. 3/27/2015-3/28/2015

   Smith SA. *CEST: Applications and implications for clinical evaluation of neurological diseases*. PennCEST 2015, Philadelphia PA. 10/25/2015 - 10/28/2015

   5. Abstracts: 2 abstracts to the American Academy of Neurology have been submitted this year (1) Conrad BN, Pawate S, Smith SA. *Functional Reorganization in Multiple Sclerosis at 7T: Altered connectivity and Relationships to Cognitive Impairment, 2)* Dula AN, Pawate S, Lyttle BD, Conrad BN, Smith SA. *Measures of Glutamate using Chemical Exchange Saturation Transfer (CEST) MRI Related*

to Cognition), 1 abstract to the Frontiers of Biomedical Imaging Science V Conference (Alex K. Smith - Characterization of the Optic Nerve in vivo using High-resolution APT-CEST), and 1 abstract presented at the annual VUIIS retreat (Conrad B, Dethrage LM, Pawate S, Smith SA. *Alterations of Resting State Functional Connectivity in Multiple Sclerosis at 7T)*

INVENTIONS, PATENTS AND LICENSES:

Nothing to Report

REPORTABLE OUTCOMES:

1. APT CEST asymmetry shows differences between healthy and MS cohorts
2. GluCEST shows differences between the healthy and MS cohorts, and additionally shows a bimodal distribution in MS cohorts indicating that in some GM, gluCEST is normal, and in others, abnormal. fMRI-driven ROI's will shed light on this distribution disparity.
3. qMT-PSR showed that 1) PSR P0 and FWHM is different in WM between cohorts, and FWHM in GM (indicating greater variance across the patients) is significantly different between MS and healthy volunteers. The median does not show a significant difference.
4. Resting-state fMRI shows regions of increased and decreased functional connectivity in patients. We believe this is the first demonstration of resting-state fMRI connectivity disparity in MS at high field.
5. Significant differences on neuropsychiatric evaluations are noted between healthy volunteers and MS patients regardless of disease duration, noted cognitive impairment, or lesion burden.

OTHER ACHIEVEMENTS:

1. Dissemination to other anatomies and other research groups has resulted in excellent collaborations
2. Performing this particular 7T MRI battery in 37 patients with MS has been leveraged with Philips medical systems to study more carefully the opportunity for 7T to be utilized in a clinical fashion, similar to what has been announced by Siemens Medical this year.
3. Interview with the primary media outlet in South Korea regarding the applicability of CEST to be deployed in patient populations (http://biz.chosun.com/site/data/html_dir/2015/03/29/2015032901804.html)
4. Database of neuropsychiatric evaluations for patients have been leveraged for multiple grant applications to be submitted by Dr. Pawate, Dr. Smith, and Dr. Bagnato (neurology) during the EWOF
5. Collaborations internal to Vanderbilt have asked to perform qMT and CEST in their patient populations as a direct result of the success of this project.
6. The transition of the CEST and qMT to lower field strength in other anatomies has been leveraged for a successful National MS Society Grant to study the spinal cord in the same patient populations.
7. I have been asked to present at patient advocacy meetings through the National MS society to discuss the potential for high field (7T) to offer new insight to clinicians seeking alternative imaging methods (3/2016)

REFERENCES: *List all references pertinent to the report using a standard journal format (i.e. format used in Science, Military Medicine, etc.)*

1. Cai K, Haris M, Singh A, Kogan F, Greenberg JH, Hariharan H, Detre JA, Reddy R. Magnetic resonance imaging of glutamate. Nature medicine 2012;18(2):302-306.3274604
2. Cai K, Singh A, Roalf DR, Nanga RP, Haris M, Hariharan H, Gur R, Reddy R. Mapping glutamate in subcortical brain structures using high-resolution GluCEST MRI. NMR in biomedicine 2013;26(10):1278-1284.3999922

APPENDICES

Appendix 1

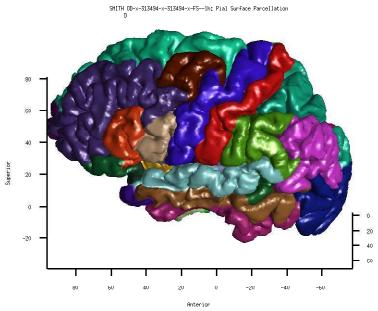
Superior
Anterior

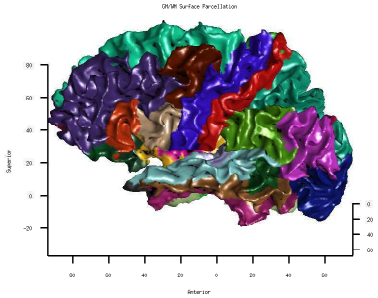
Superior
Anterior

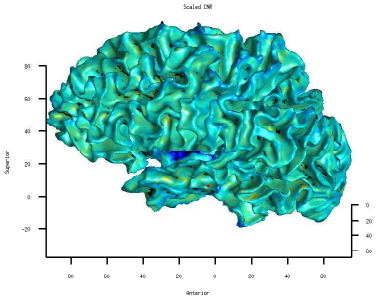
Superior
Anterior

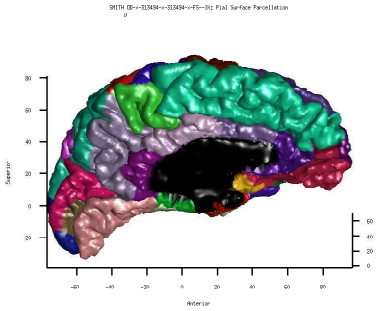
Superior
Anterior

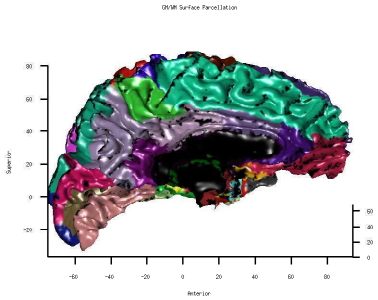
Superior
Anterior

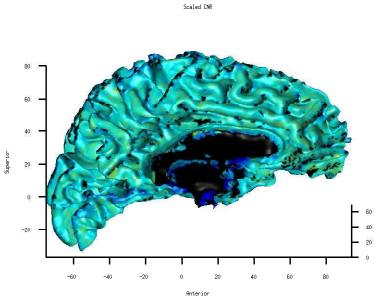
Superior
Anterior

SMITH$_D$OD−x−313494−x−313494−x−FS−−lh: GM/WM Contrast to Noise Ratio By Region

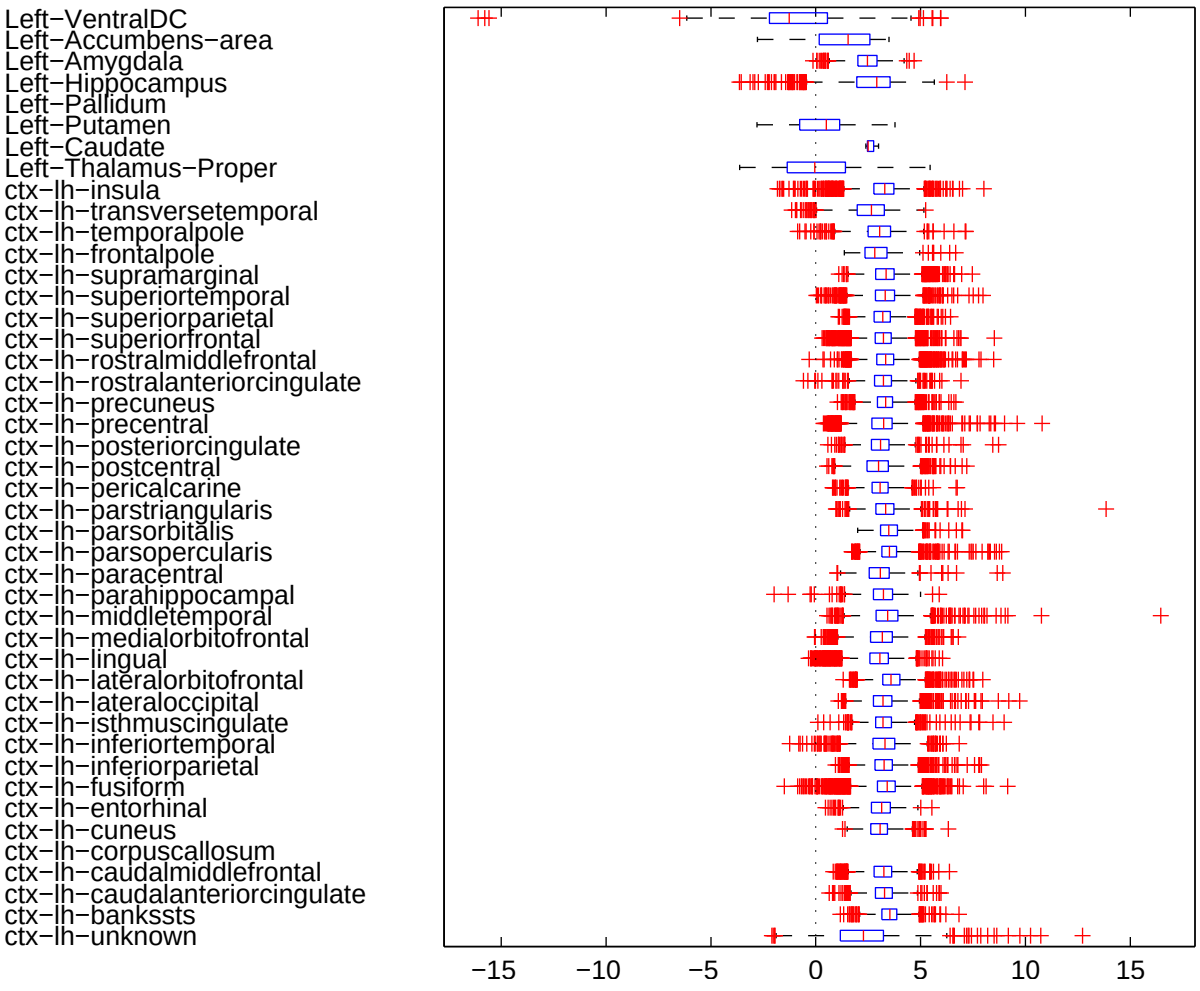

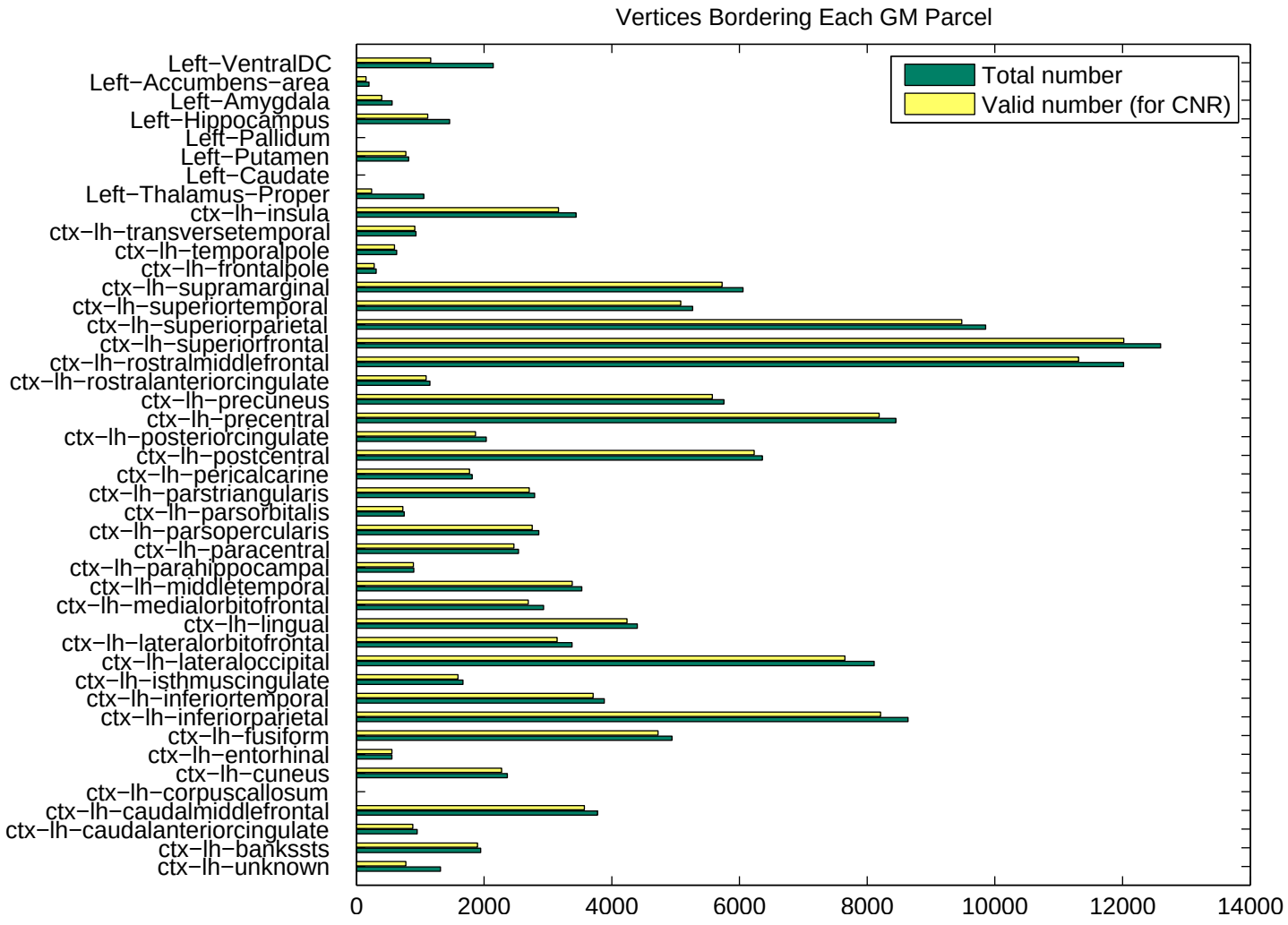
Vertices Bordering Each GM Parcel
Total number
Valid number (for CNR)
Left−VentralDC
Left−Accumbens−area
Left−Amygdala
Left−Hippocampus
Left−Pallidum
Left−Putamen
Left−Caudate
Left−Thalamus−Proper
ctx−lh−insula
ctx−lh−transversetemporal
ctx−lh−temporalpole
ctx−lh−frontalpole
ctx−lh−supramarginal
ctx−lh−superiortemporal
ctx−lh−superiorparietal
ctx−lh−superiorfrontal
ctx−lh−rostralmiddlefrontal
ctx−lh−rostralanteriorcingulate
ctx−lh−precuneus
ctx−lh−precentral
ctx−lh−posteriorcingulate
ctx−lh−postcentral
ctx−lh−pericalcarine
ctx−lh−parstriangularis
ctx−lh−parsorbitalis
ctx−lh−parsopercularis
ctx−lh−paracentral
ctx−lh−parahippocampal
ctx−lh−middletemporal
ctx−lh−medialorbitofrontal
ctx−lh−lingual
ctx−lh−lateralorbitofrontal
ctx−lh−lateraloccipital
ctx−lh−isthmuscingulate
ctx−lh−inferiortemporal
ctx−lh−inferiorparietal
ctx−lh−fusiform
ctx−lh−entorhinal
ctx−lh−cuneus
ctx−lh−corpuscallosum
ctx−lh−caudalmiddlefrontal
ctx−lh−caudalanteriorcingulate
ctx−lh−bankssts
ctx−lh−unknown
0
2000
4000
6000
8000
10000
12000
14000

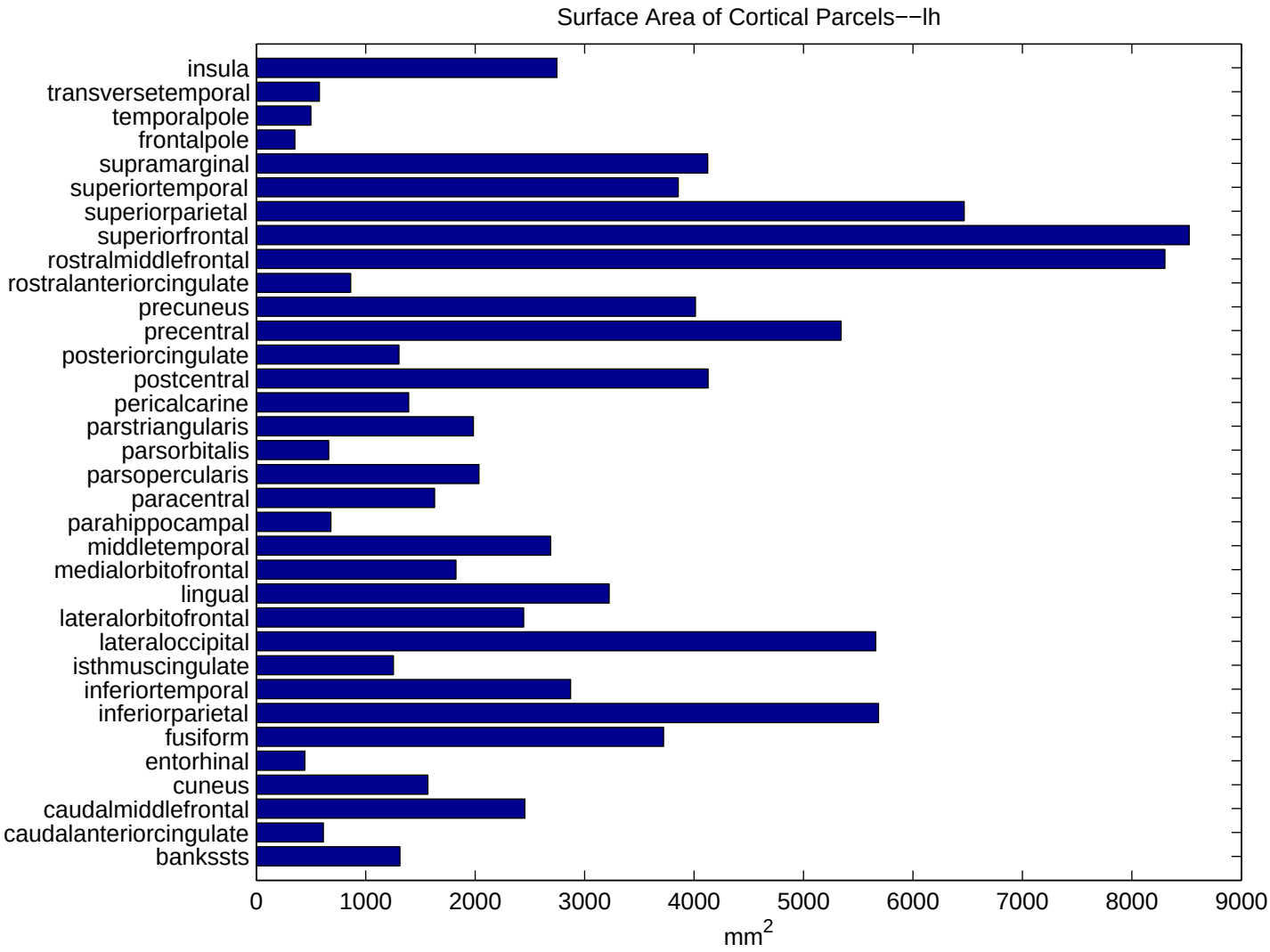
Surface Area of Cortical Parcels−−lh
insula
transversetemporal
temporalpole
frontalpole
supramarginal
superiortemporal
superiorparietal
superiorfrontal
rostralmiddlefrontal
rostralanteriorcingulate
precuneus
precentral
posteriorcingulate
postcentral
pericalcarine
parstriangularis
parsorbitalis
parsopercularis
paracentral
parahippocampal
middletemporal
medialorbitofrontal
lingual
lateralorbitofrontal
lateraloccipital
isthmuscingulate
inferiortemporal
inferiorparietal
fusiform
entorhinal
cuneus
caudalmiddlefrontal
caudalanteriorcingulate
bankssts
0
1000
2000
3000
4000
5000
6000
7000
8000
9000
mm2

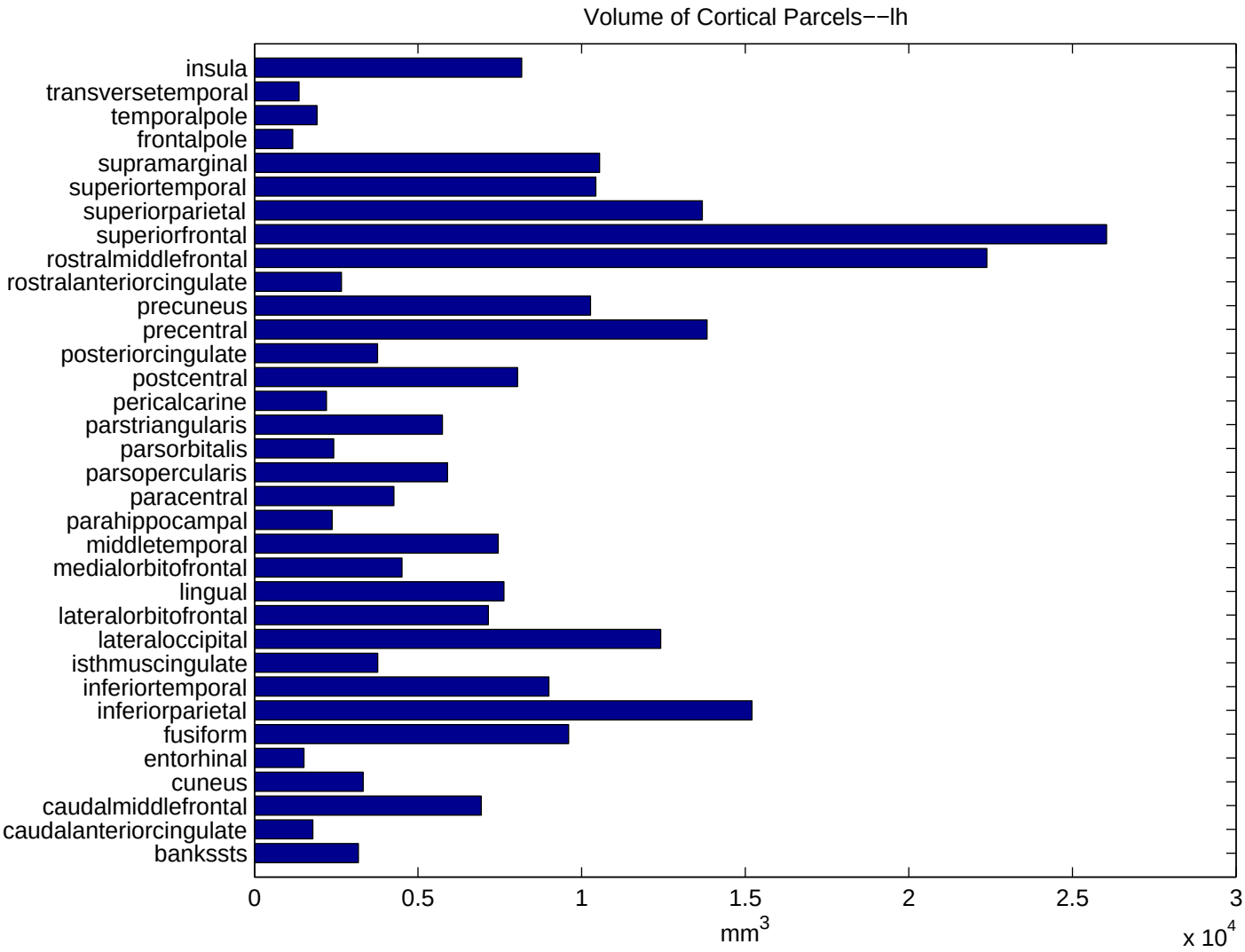
Volume of Cortical Parcels−−lh
insula
transversetemporal
temporalpole
frontalpole
supramarginal
superiortemporal
superiorparietal
superiorfrontal
rostralmiddlefrontal
rostralanteriorcingulate
precuneus
precentral
posteriorcingulate
postcentral
pericalcarine
parstriangularis
parsorbitalis
parsopercularis
paracentral
parahippocampal
middletemporal
medialorbitofrontal
lingual
lateralorbitofrontal
lateraloccipital
isthmuscingulate
inferiortemporal
inferiorparietal
fusiform
entorhinal
cuneus
caudalmiddlefrontal
caudalanteriorcingulate
bankssts
0
0.5
1
1.5
2
2.5
3
mm3
x 10^4

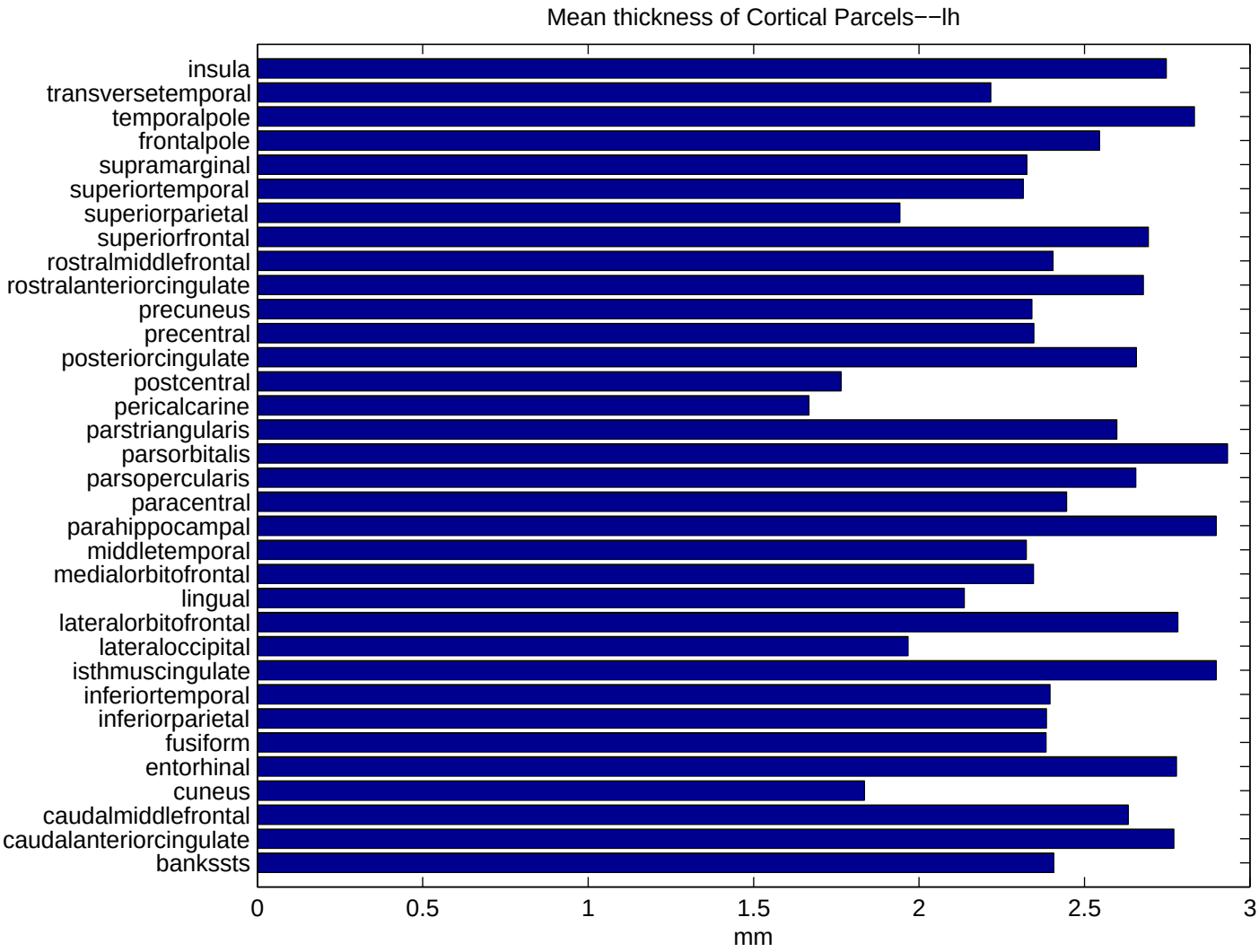
Mean thickness of Cortical Parcels−−lh
insula
transversetemporal
temporalpole
frontalpole
supramarginal
superiortemporal
superiorparietal
superiorfrontal
rostralmiddlefrontal
rostralanteriorcingulate
precuneus
precentral
posteriorcingulate
postcentral
pericalcarine
parstriangularis
parsorbitalis
parsopercularis
paracentral
parahippocampal
middletemporal
medialorbitofrontal
lingual
lateralorbitofrontal
lateraloccipital
isthmuscingulate
inferiortemporal
inferiorparietal
fusiform
entorhinal
cuneus
caudalmiddlefrontal
caudalanteriorcingulate
bankssts
0
0.5
1
1.5
2
2.5
3
mm

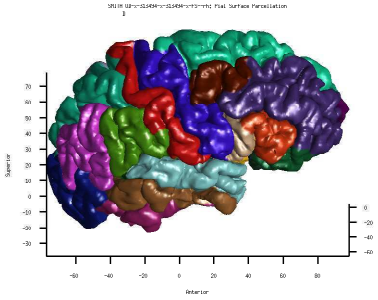
Superior
Anterior

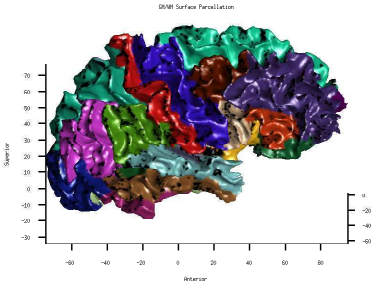
DKAM Surface Parcellation
Superior
Anterior

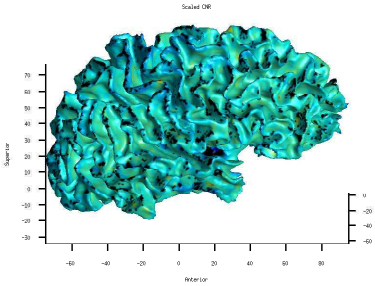
Scaled CNR
Superior
Anterior

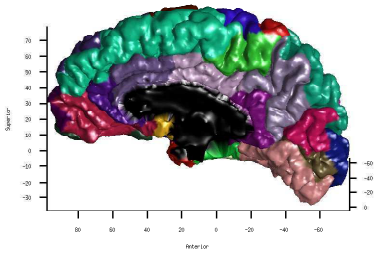
Superior
Anterior

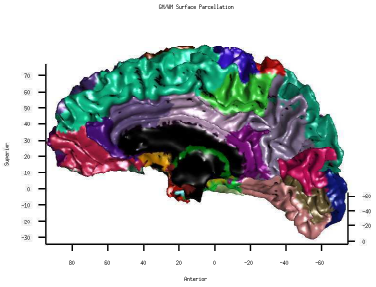
DKAM Surface Parcellation
Superior
Anterior

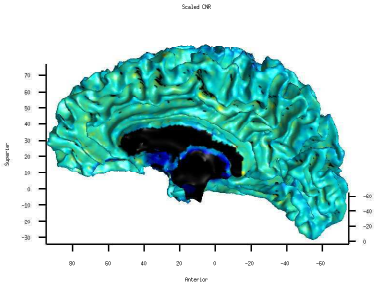
Scaled CNR
Superior
Anterior

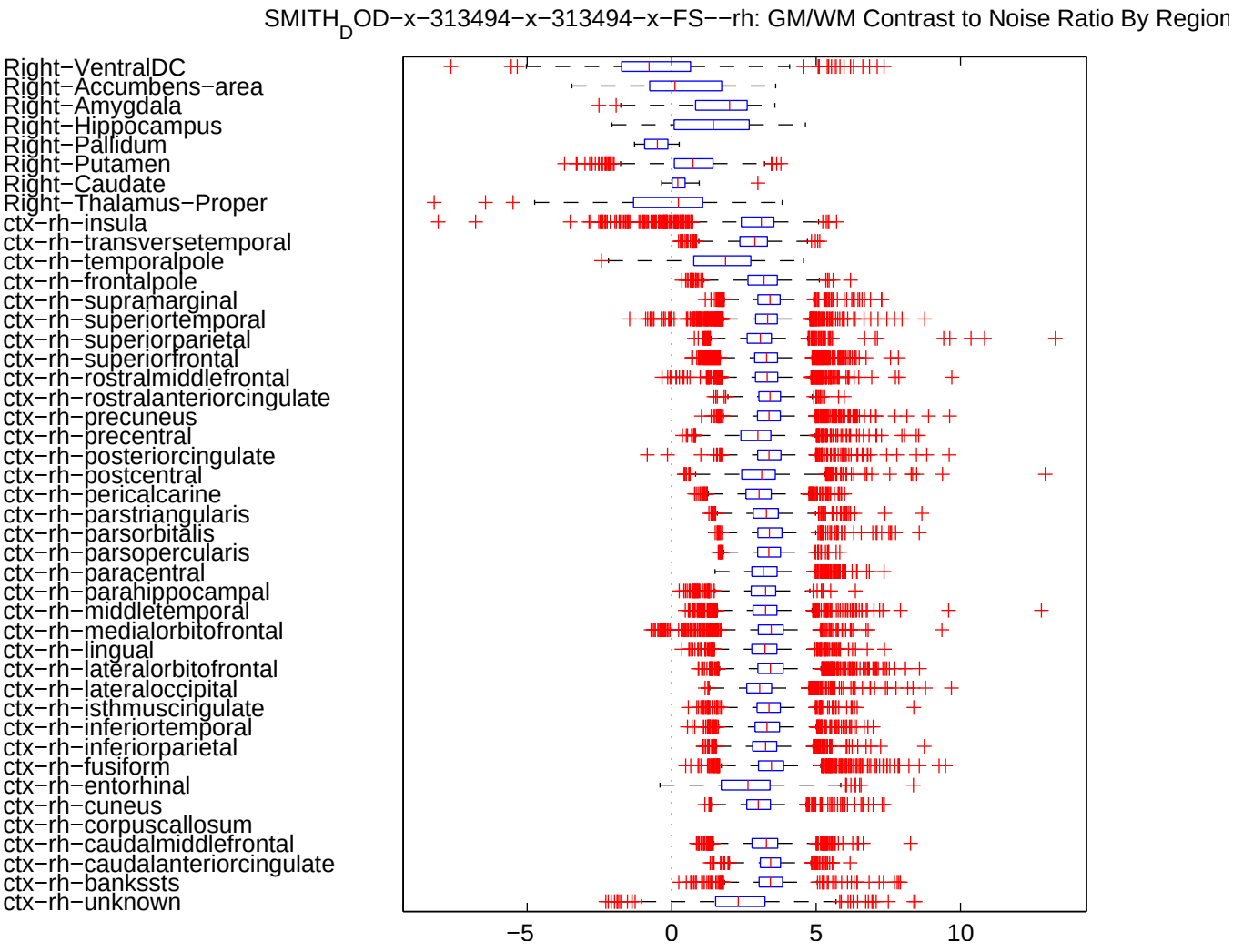
SMITH_DOD−x−313494−x−313494−x−FS−−rh: GM/WM Contrast to Noise Ratio By Region
Right−VentralDC
Right−Accumbens−area
Right−Amygdala
Right−Hippocampus
Right−Pallidum
Right−Putamen
Right−Caudate
Right−Thalamus−Proper
ctx−rh−insula
ctx−rh−transversetemporal
ctx−rh−temporalpole
ctx−rh−frontalpole
ctx−rh−supramarginal
ctx−rh−superiortemporal
ctx−rh−superiorparietal
ctx−rh−superiorfrontal
ctx−rh−rostralmiddlefrontal
ctx−rh−rostralanteriorcingulate
ctx−rh−precuneus
ctx−rh−precentral
ctx−rh−posteriorcingulate
ctx−rh−postcentral
ctx−rh−pericalcarine
ctx−rh−parstriangularis
ctx−rh−parsorbitalis
ctx−rh−parsopercularis
ctx−rh−paracentral
ctx−rh−parahippocampal
ctx−rh−middletemporal
ctx−rh−medialorbitofrontal
ctx−rh−lingual
ctx−rh−lateralorbitofrontal
ctx−rh−lateraloccipital
ctx−rh−isthmuscingulate
ctx−rh−inferiortemporal
ctx−rh−inferiorparietal
ctx−rh−fusiform
ctx−rh−entorhinal
ctx−rh−cuneus
ctx−rh−corpuscallosum
ctx−rh−caudalmiddlefrontal
ctx−rh−caudalanteriorcingulate
ctx−rh−bankssts
ctx−rh−unknown
−5
0
5
10

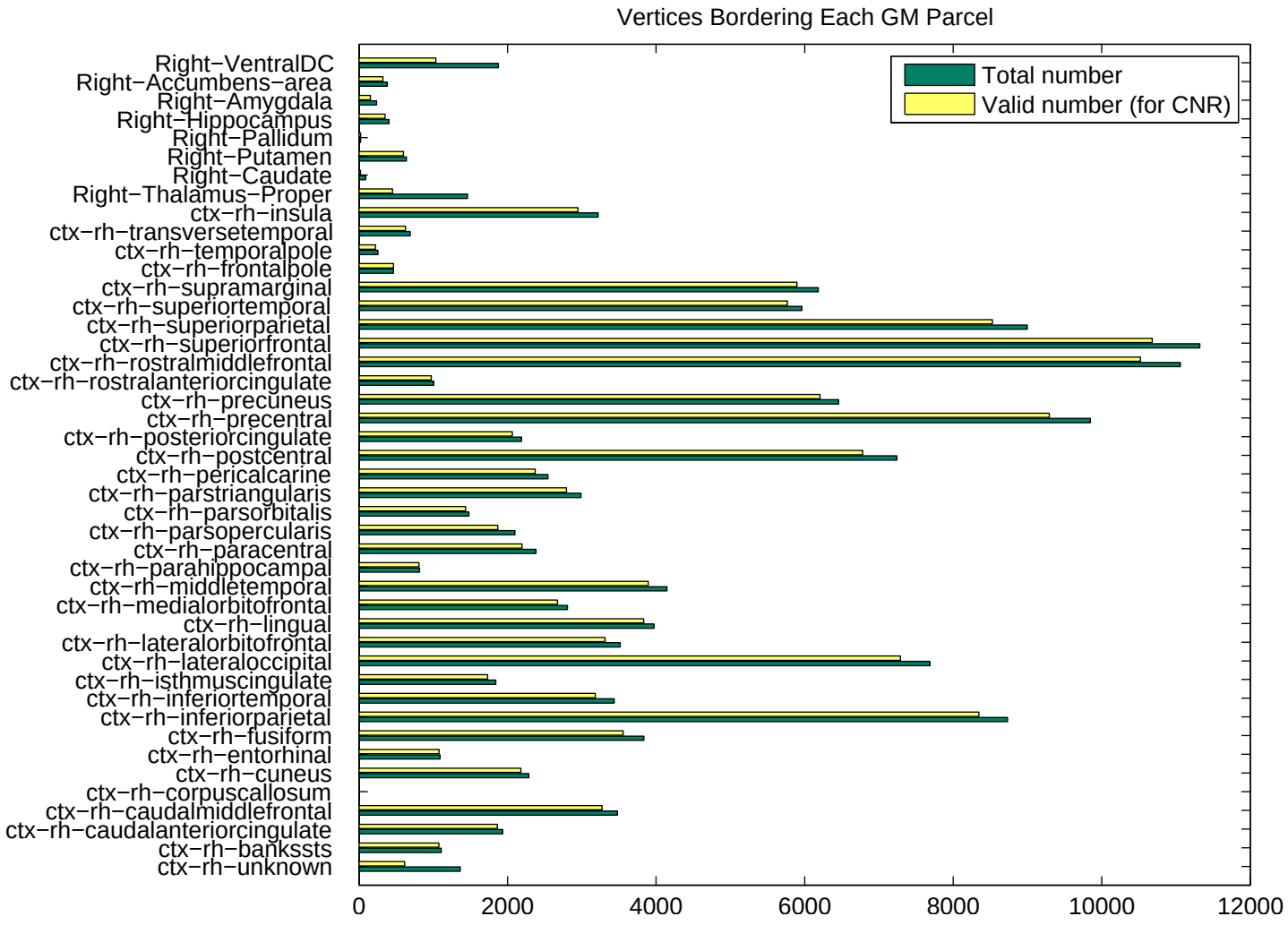
Vertices Bordering Each GM Parcel
Total number
Valid number (for CNR)
Right−VentralDC
Right−Accumbens−area
Right−Amygdala
Right−Hippocampus
Right−Pallidum
Right−Putamen
Right−Caudate
Right−Thalamus−Proper
ctx−rh−insula
ctx−rh−transversetemporal
ctx−rh−temporalpole
ctx−rh−frontalpole
ctx−rh−supramarginal
ctx−rh−superiortemporal
ctx−rh−superiorparietal
ctx−rh−superiorfrontal
ctx−rh−rostralmiddlefrontal
ctx−rh−rostralanteriorcingulate
ctx−rh−precuneus
ctx−rh−precentral
ctx−rh−posteriorcingulate
ctx−rh−postcentral
ctx−rh−pericalcarine
ctx−rh−parstriangularis
ctx−rh−parsorbitalis
ctx−rh−parsopercularis
ctx−rh−paracentral
ctx−rh−parahippocampal
ctx−rh−middletemporal
ctx−rh−medialorbitofrontal
ctx−rh−lingual
ctx−rh−lateralorbitofrontal
ctx−rh−lateraloccipital
ctx−rh−isthmuscingulate
ctx−rh−inferiortemporal
ctx−rh−inferiorparietal
ctx−rh−fusiform
ctx−rh−entorhinal
ctx−rh−cuneus
ctx−rh−corpuscallosum
ctx−rh−caudalmiddlefrontal
ctx−rh−caudalanteriorcingulate
ctx−rh−bankssts
ctx−rh−unknown
0
2000
4000
6000
8000
10000
12000

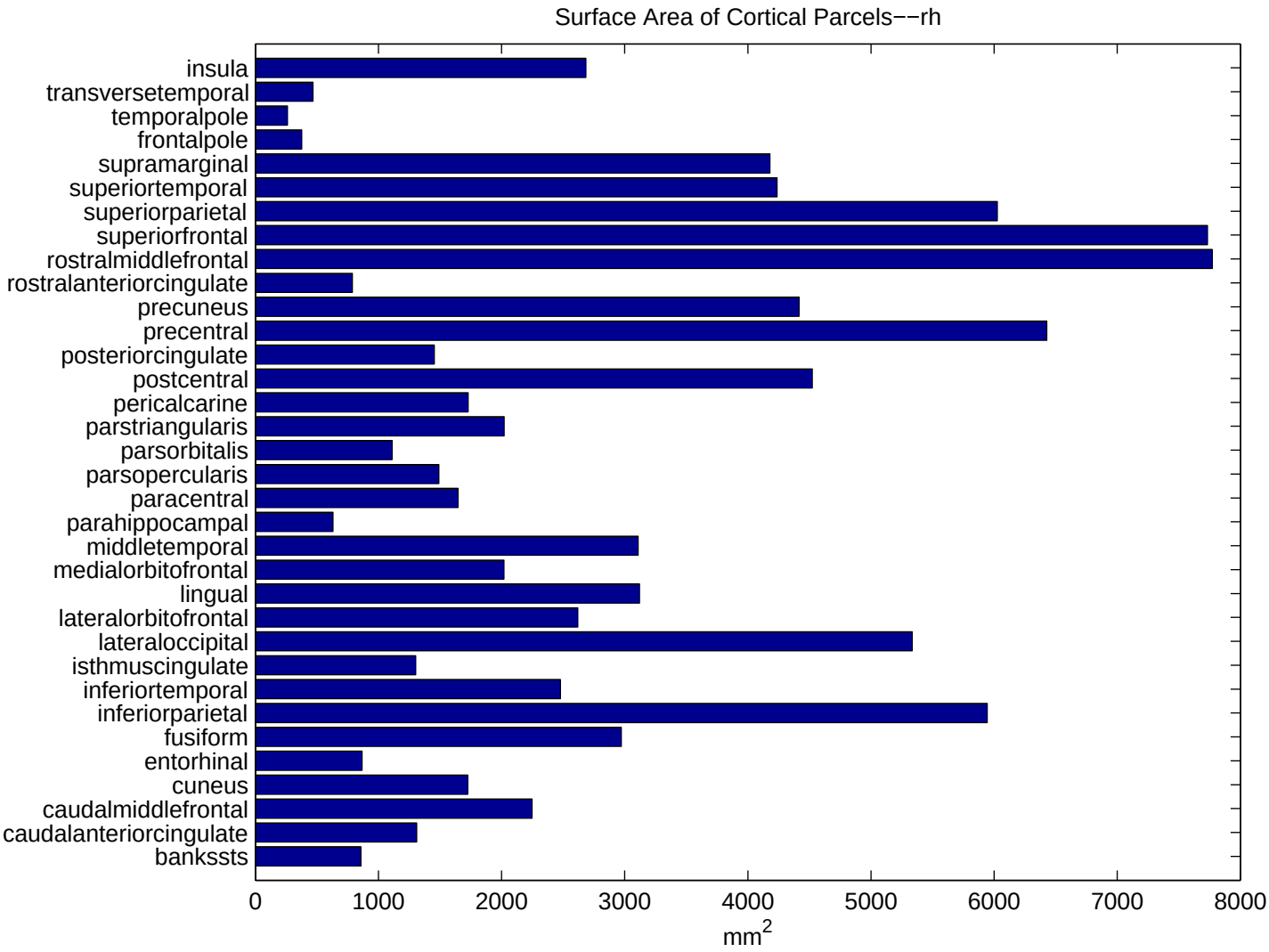
Surface Area of Cortical Parcels−−rh
insula
transversetemporal
temporalpole
frontalpole
supramarginal
superiortemporal
superiorparietal
superiorfrontal
rostralmiddlefrontal
rostralanteriorcingulate
precuneus
precentral
posteriorcingulate
postcentral
pericalcarine
parstriangularis
parsorbitalis
parsopercularis
paracentral
parahippocampal
middletemporal
medialorbitofrontal
lingual
lateralorbitofrontal
lateraloccipital
isthmuscingulate
inferiortemporal
inferiorparietal
fusiform
entorhinal
cuneus
caudalmiddlefrontal
caudalanteriorcingulate
bankssts
0
1000
2000
3000
4000
5000
6000
7000
8000
mm2

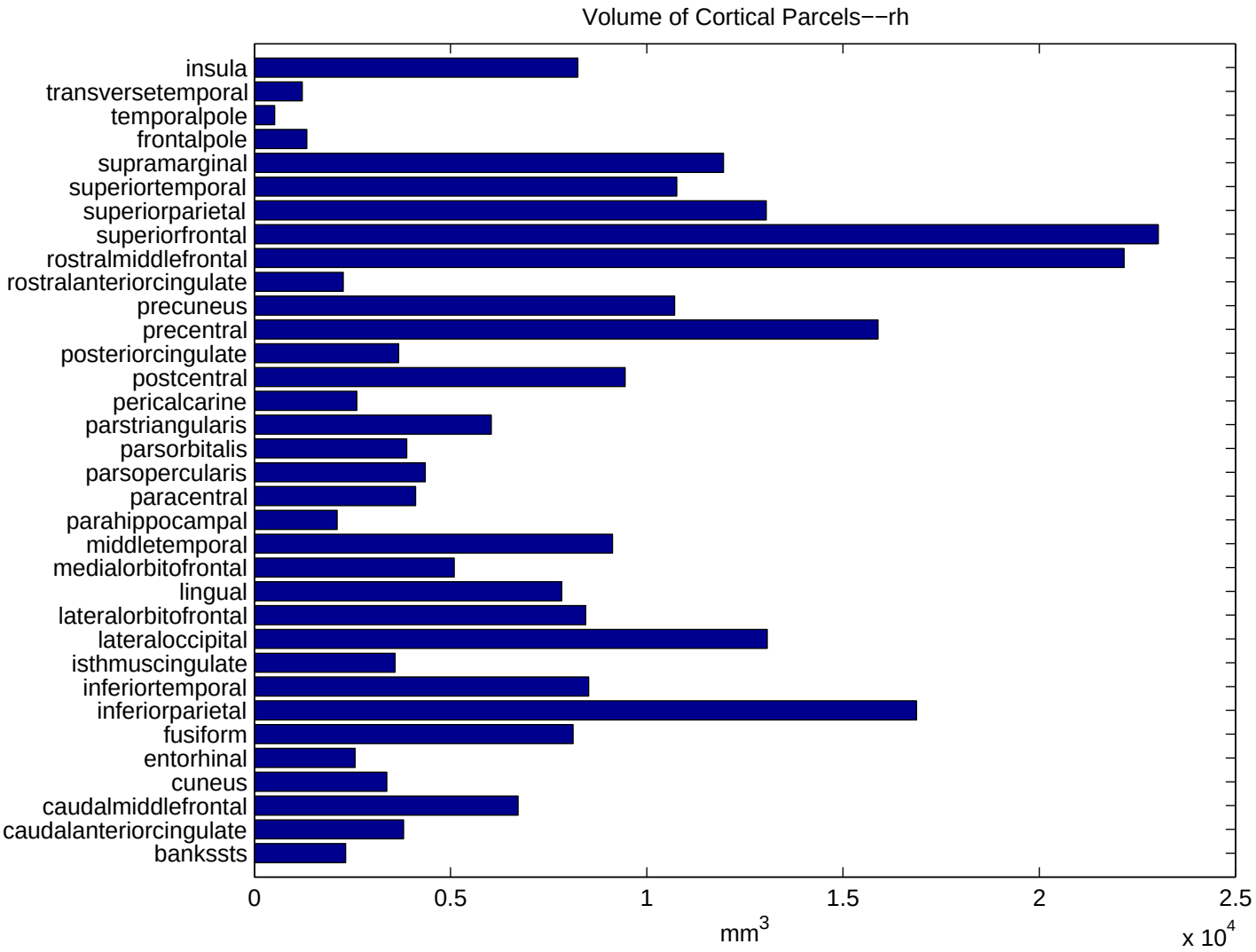
Volume of Cortical Parcels−−rh
insula
transversetemporal
temporalpole
frontalpole
supramarginal
superiortemporal
superiorparietal
superiorfrontal
rostralmiddlefrontal
rostralanteriorcingulate
precuneus
precentral
posteriorcingulate
postcentral
pericalcarine
parstriangularis
parsorbitalis
parsopercularis
paracentral
parahippocampal
middletemporal
medialorbitofrontal
lingual
lateralorbitofrontal
lateraloccipital
isthmuscingulate
inferiortemporal
inferiorparietal
fusiform
entorhinal
cuneus
caudalmiddlefrontal
caudalanteriorcingulate
bankssts
0
0.5
1
1.5
2
2.5
mm3
x 10^4

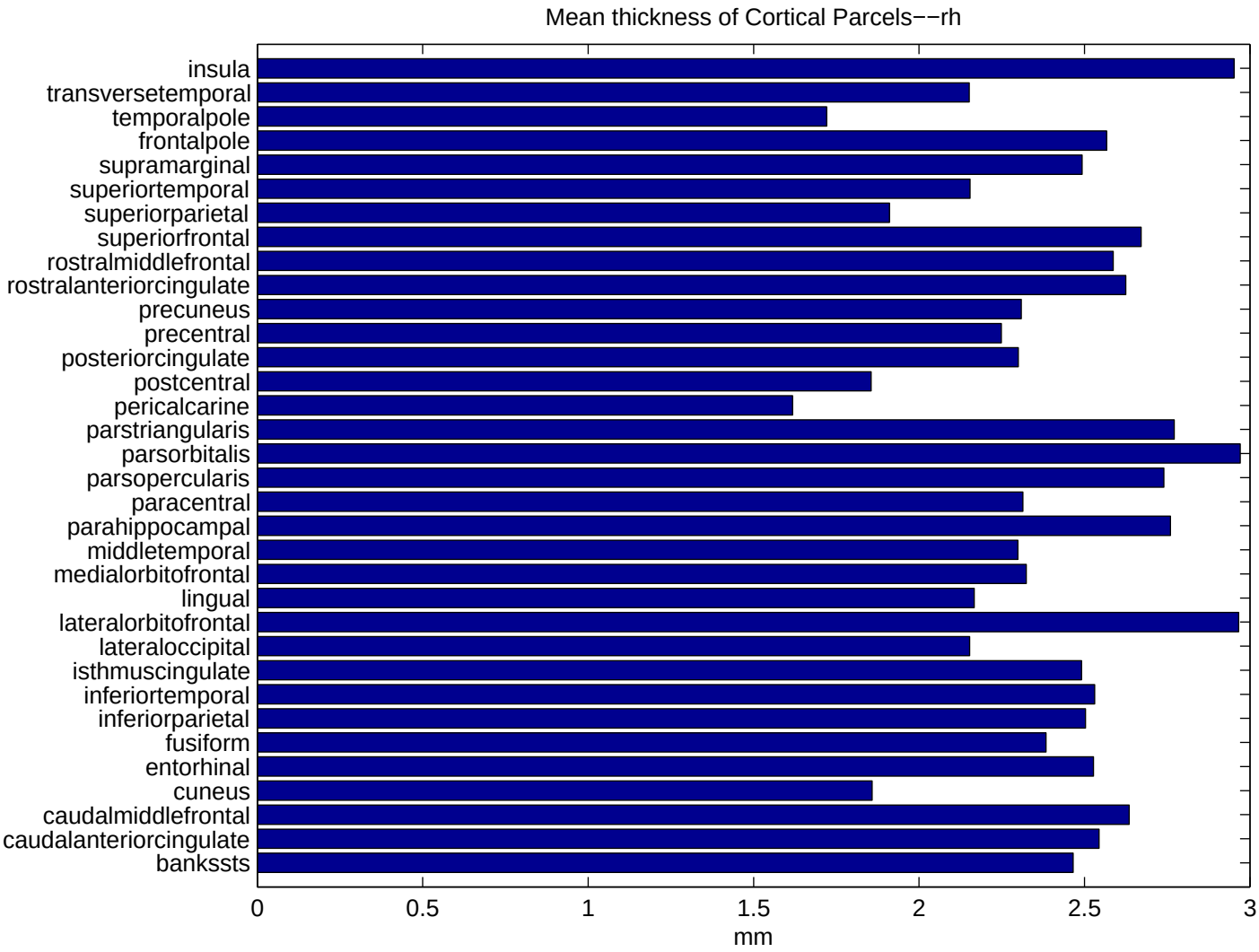
Mean thickness of Cortical Parcels−−rh
insula
transversetemporal
temporalpole
frontalpole
supramarginal
superiortemporal
superiorparietal
superiorfrontal
rostralmiddlefrontal
rostralanteriorcingulate
precuneus
precentral
posteriorcingulate
postcentral
pericalcarine
parstriangularis
parsorbitalis
parsopercularis
paracentral
parahippocampal
middletemporal
medialorbitofrontal
lingual
lateralorbitofrontal
lateraloccipital
isthmuscingulate
inferiortemporal
inferiorparietal
fusiform
entorhinal
cuneus
caudalmiddlefrontal
caudalanteriorcingulate
bankssts
0
0.5
1
1.5
2
2.5
3
mm

Multi-atlas CRUISE v1.0 09-Nov-2015

project: SMITH_DOD
subject: 313494
project: 313494
MASI Lab - Yuankai Huo
https:

Surface Overlay

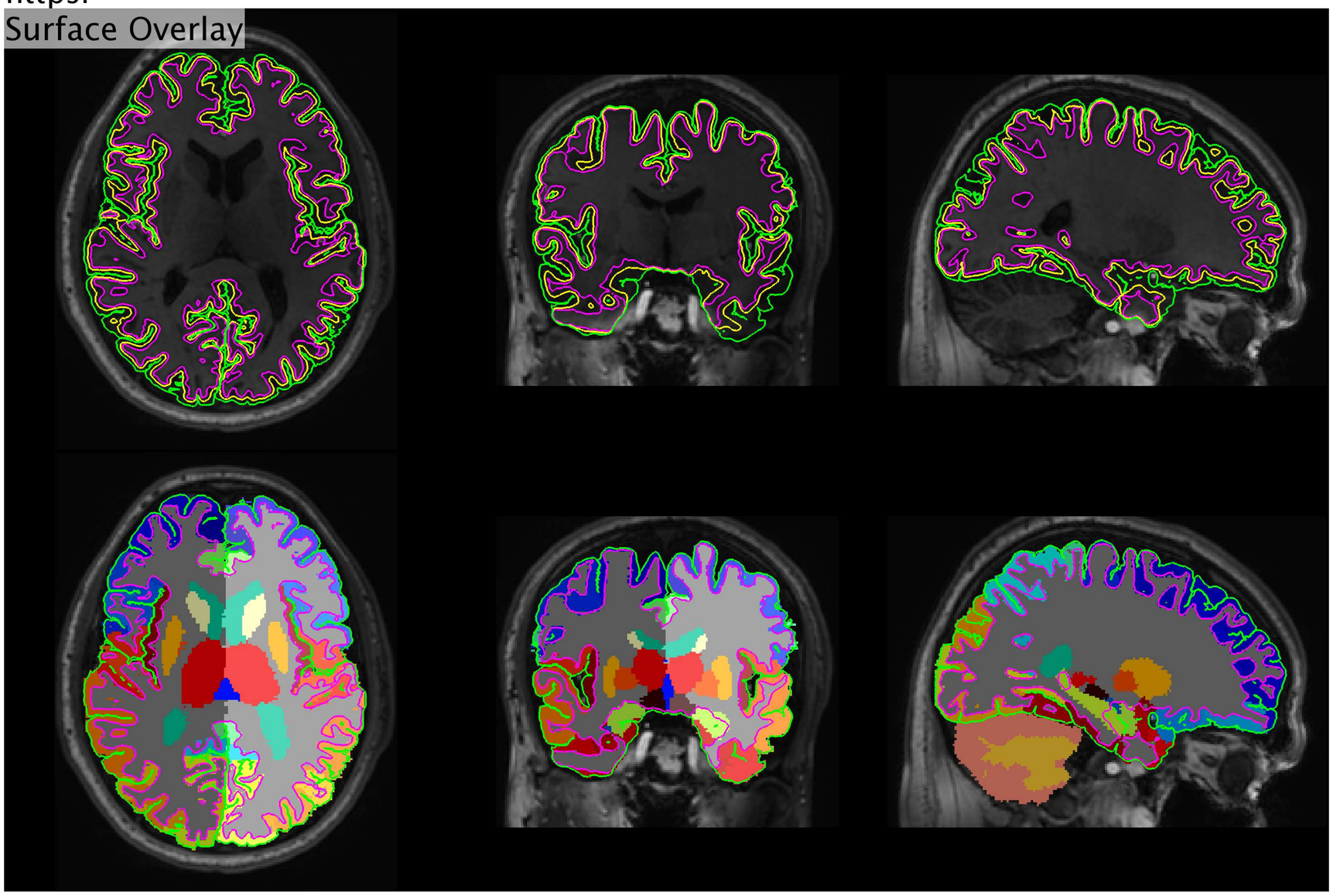

Inner Surface

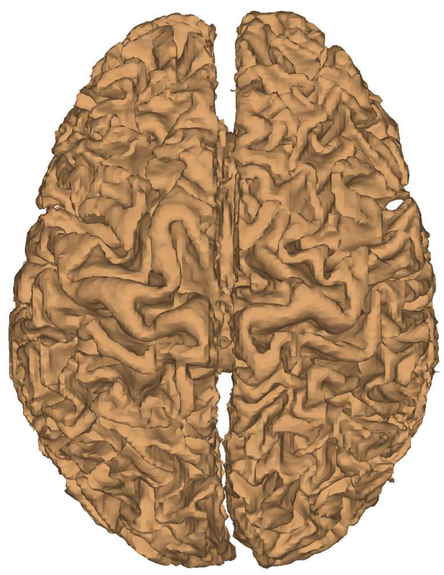

Central Surfface

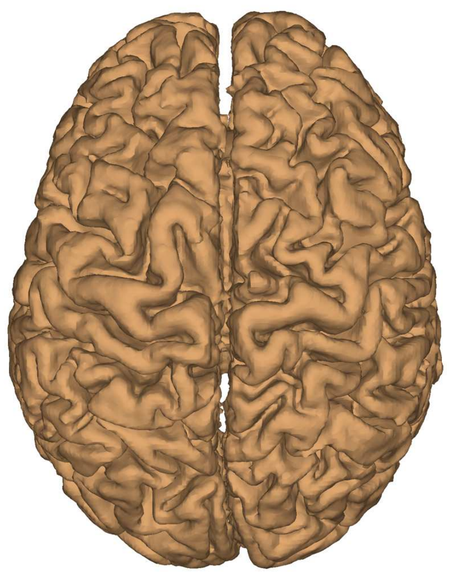

Outer Surface

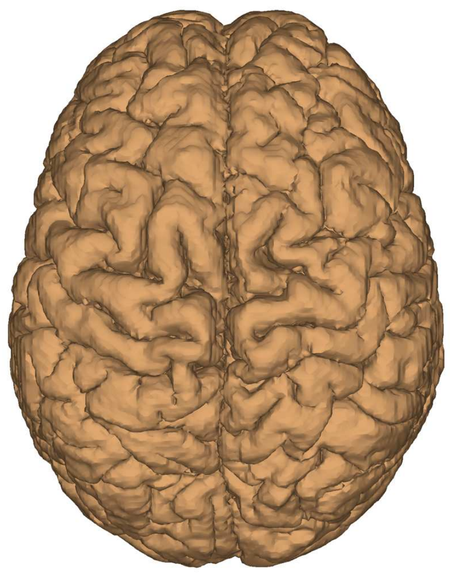

Histogram of cortical thickness

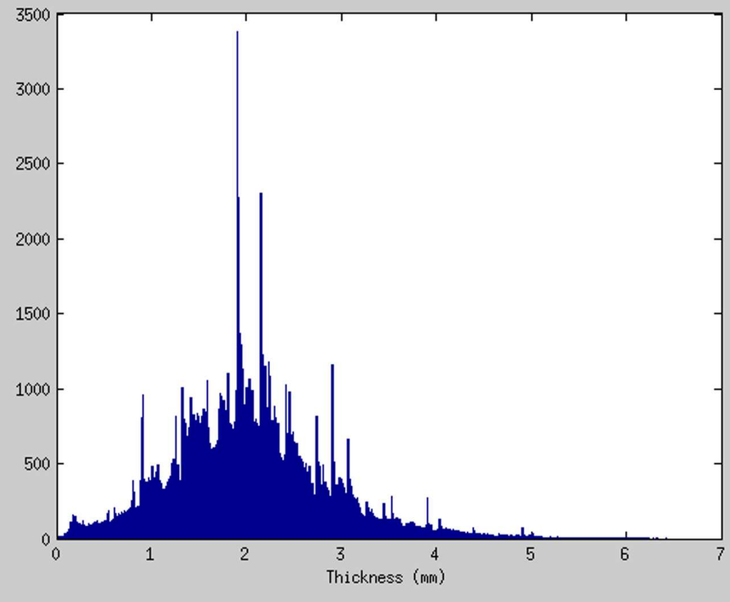

Whole Brain Multi-Atlas Segmentation Results

Project:	SMITH_DOD	Subject:	313494	Experiment:	313494

	Axial	Coronal	Saggital
Raw Image	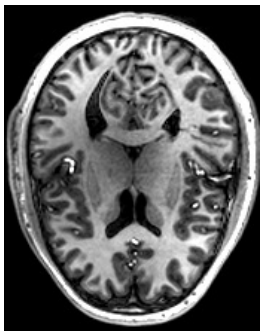	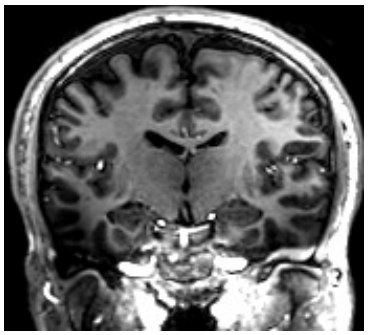	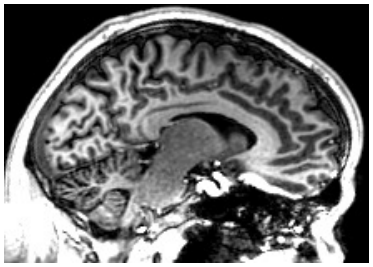
Slicewise Segmentation	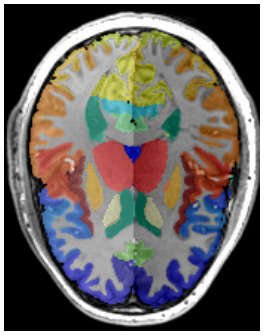	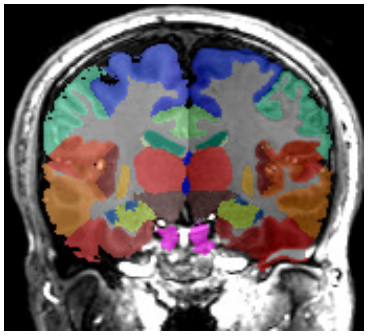	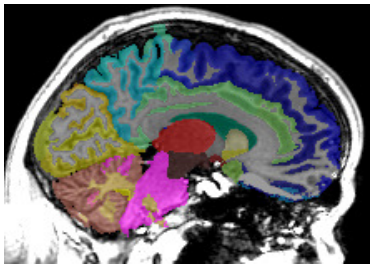
Cortical Segmentation	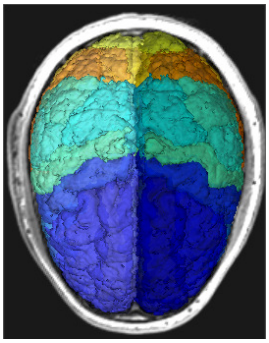	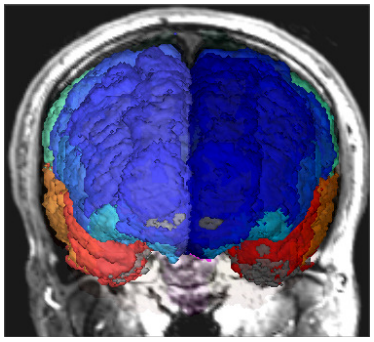	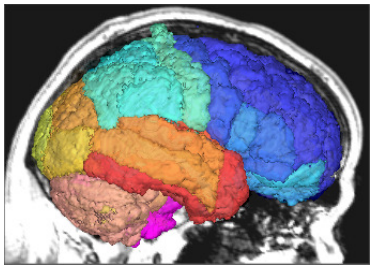
Mid-Brain Segmentation	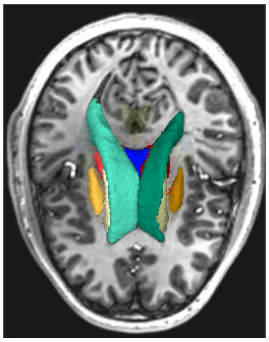	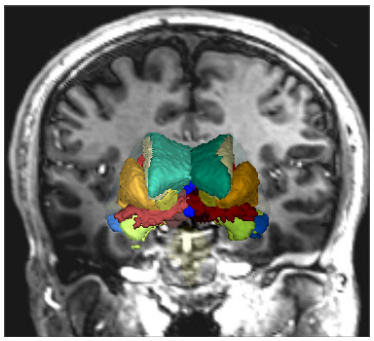	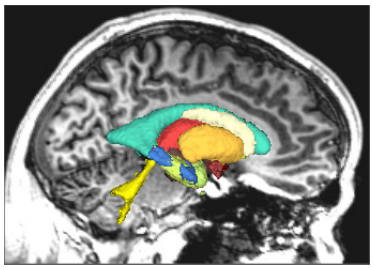

26-Sep-2015	MASI Lab - Andrew Asman	Version 1.2

https://masi.vuse.vanderbilt.edu/index.php/Image_Analysis_Software#Multi-Atlas_Segmentation_Pipeline

Segmentation: ..VBM_results/SMITH_DOD−x−313494−x−313494−x−301.nii

Versions Matlab/SPM8/VBM8:	8.1 / 5236 / 435
Non−linear normalization:	High−dimensional (Dartel)
Tissue Probability Map:	..21/scratch/mcr/spm8/toolbox/Seg/TPM.nii
Affine regularization:	mni
Warp regularisation:	4
Bias FWHM:	60
Kmeans initialization:	1
Bias FWHM in Kmeans:	60
SANLM:	yes
MRF weighting:	0.15

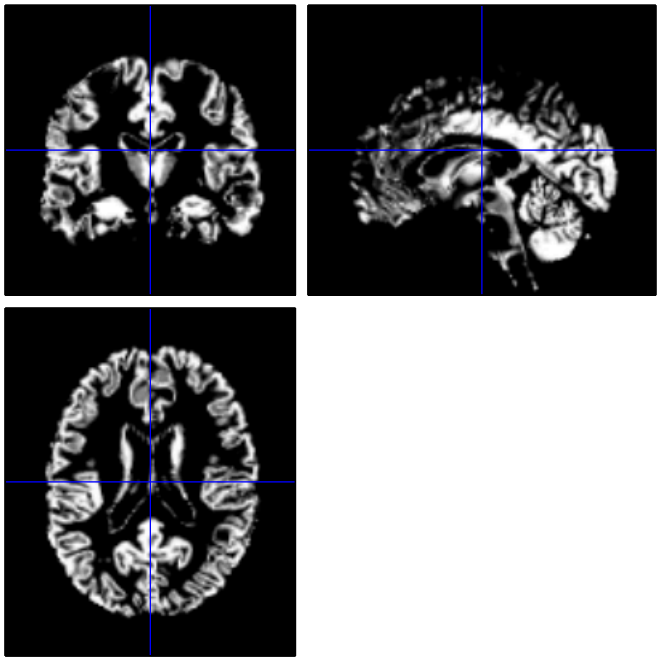

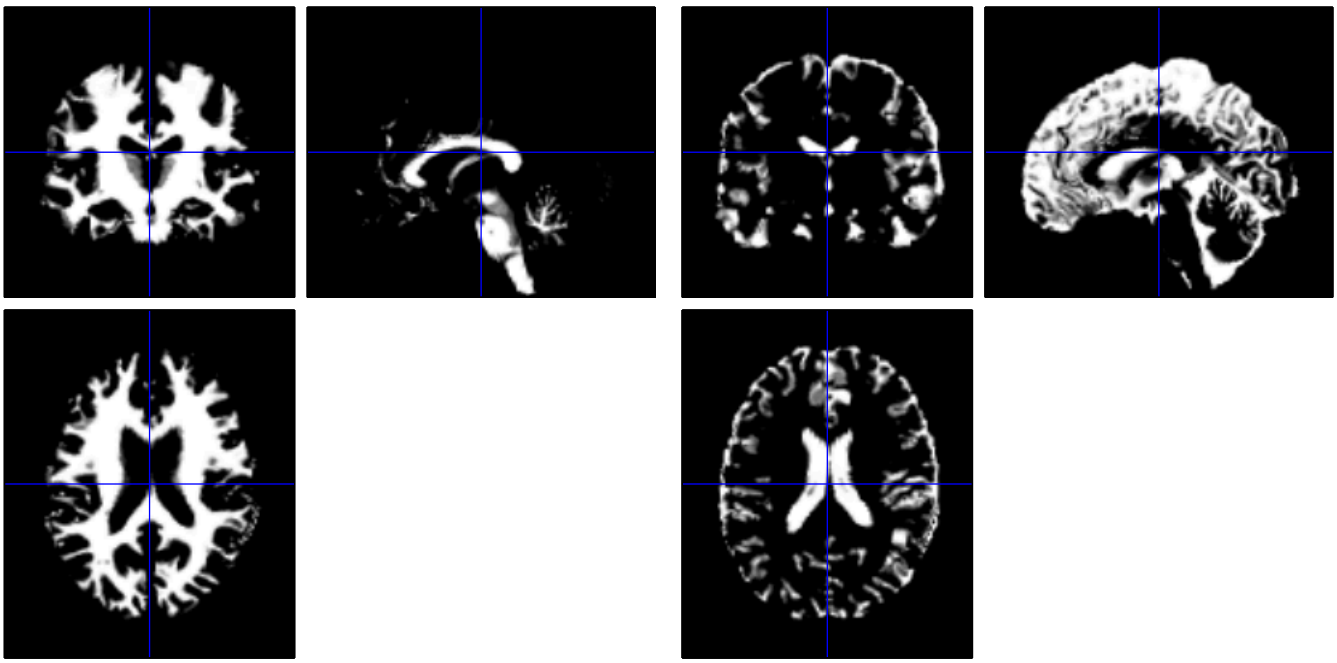

Spatial Normalisation

Image : /tmp/SMITH_DOD−x−313494−x−313494−x−301−x−VBMQA/VBM_results

Linear {affine} component
X1 = 1.109*X +0.002*Y −0.036*Z −1.285
Y1 = 0.028*X +0.950*Y +0.300*Z −18.509
Z1 = 0.031*X −0.395*Y +0.979*Z −18.556

16 nonlinear iterations
7 x 9 x 7 basis functions

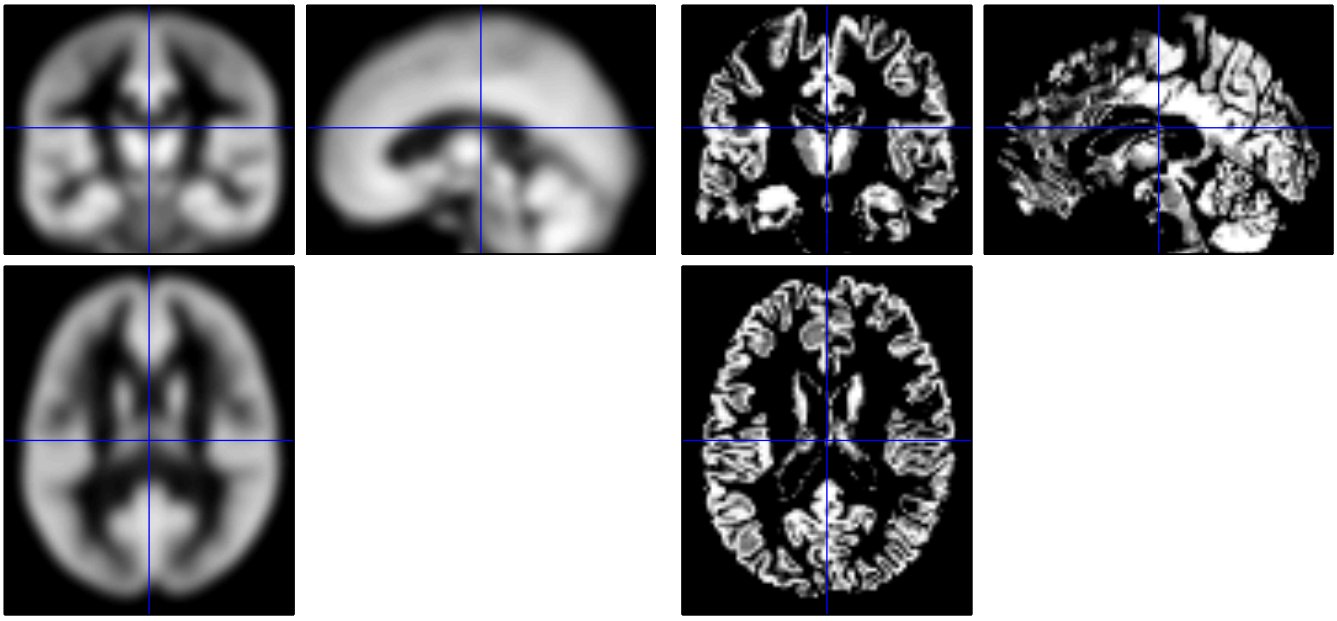

Functional MRI Quality Report (1/2)

Project: SMITH_DOD - Subject: 313494 - Session: 313494 - Scan: 901

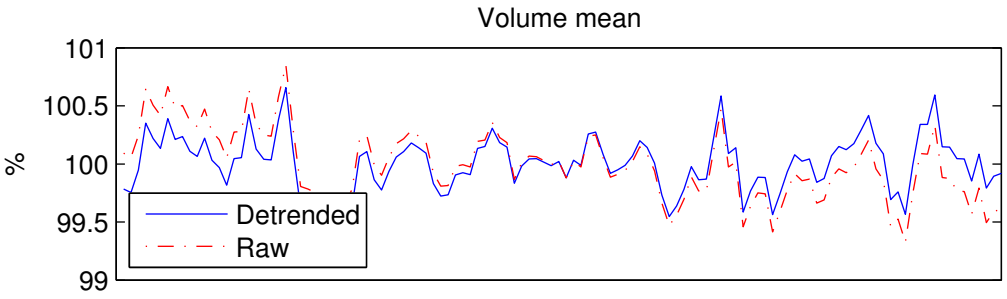

Summary:

med_tsnr = 75
glob_sd = 0.24 %
displc_99 = 0.15 mm
delta_95 = 3.97 %

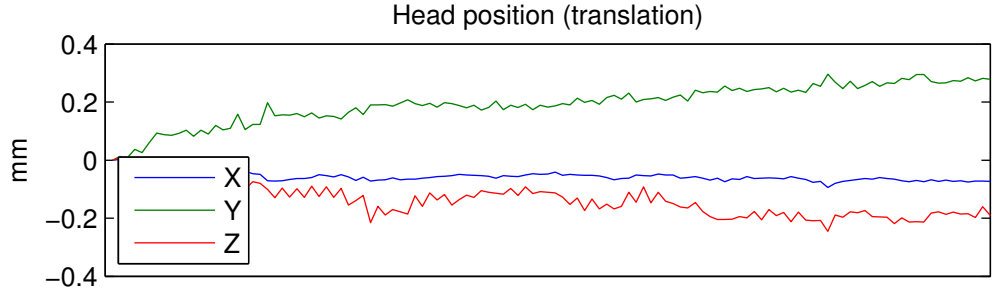

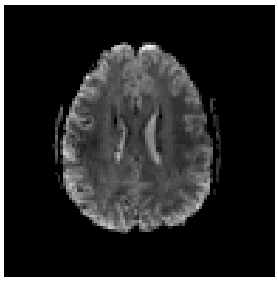

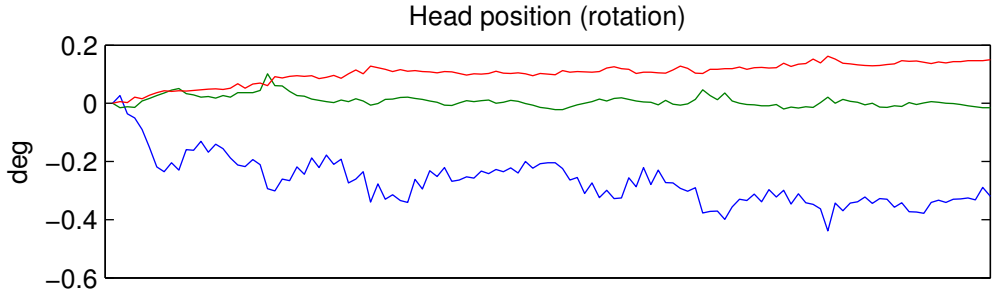

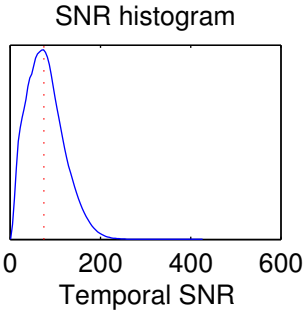

Temporal SNR:
5%tile: 20
Median: 75
95%tile: 152

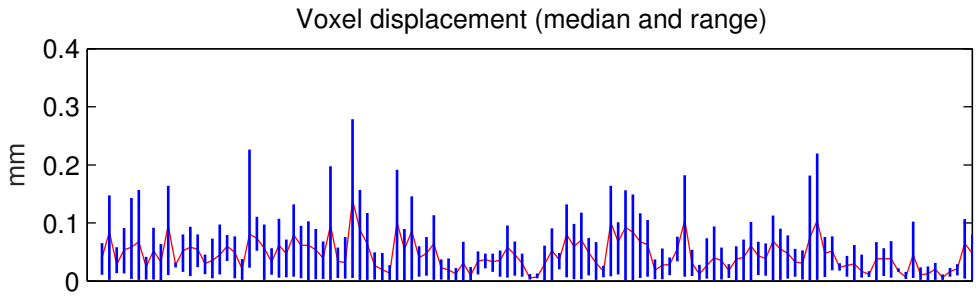

Std dev of global:
0.24 %

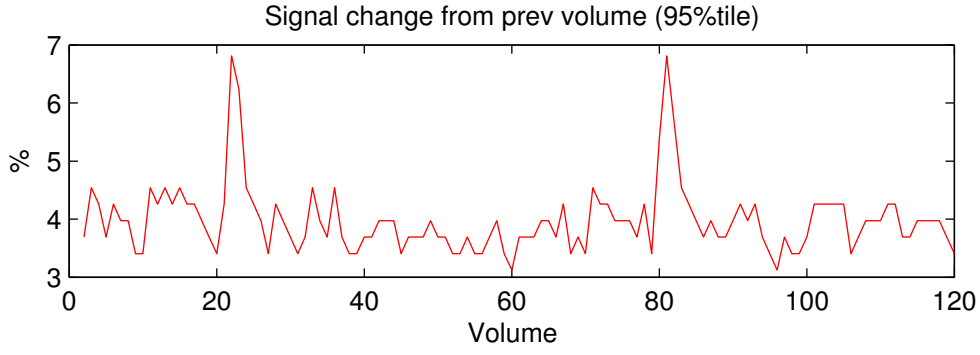

Voxel displacement:
Median: 0.04 mm
95%tile: 0.09 mm
99%tile: 0.15 mm

Signal delta:
95%tile: 3.97 %

Report date: 24-Sep-2015

Matlab version: 8.1.0.604 (R2013a)

Functional MRI Quality Report (2/2)

Project: SMITH_DOD - Subject: 313494 - Session: 313494 - Scan: 901

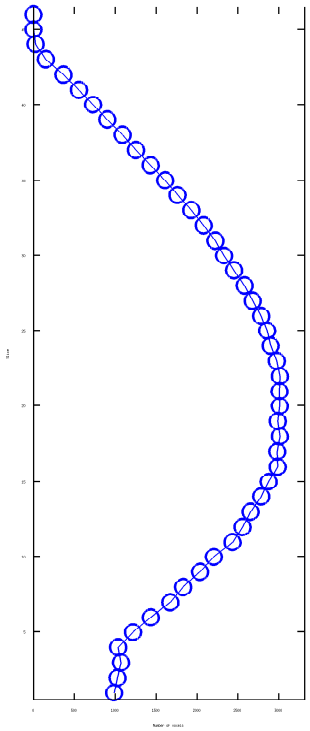

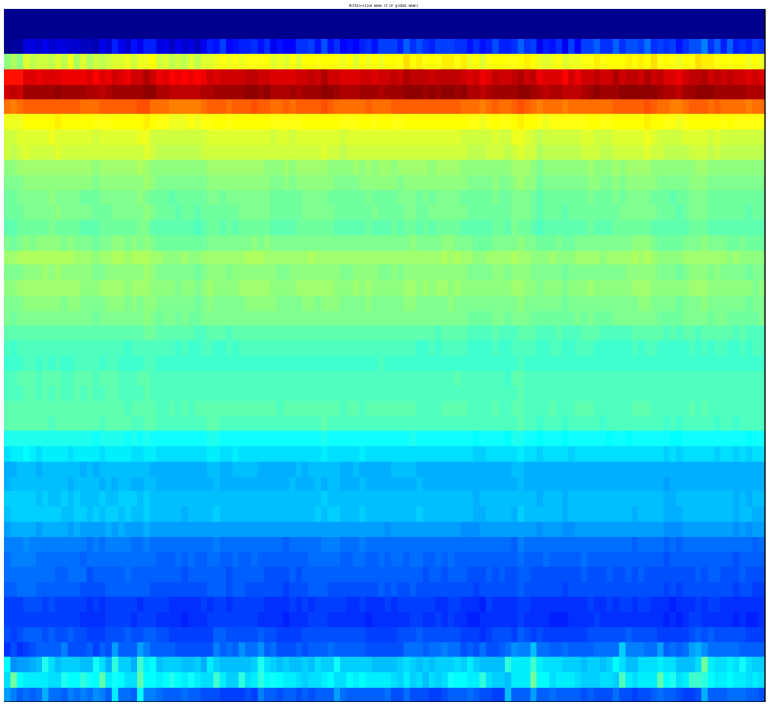

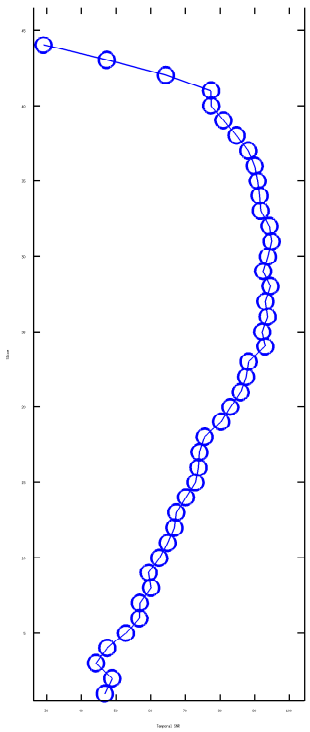

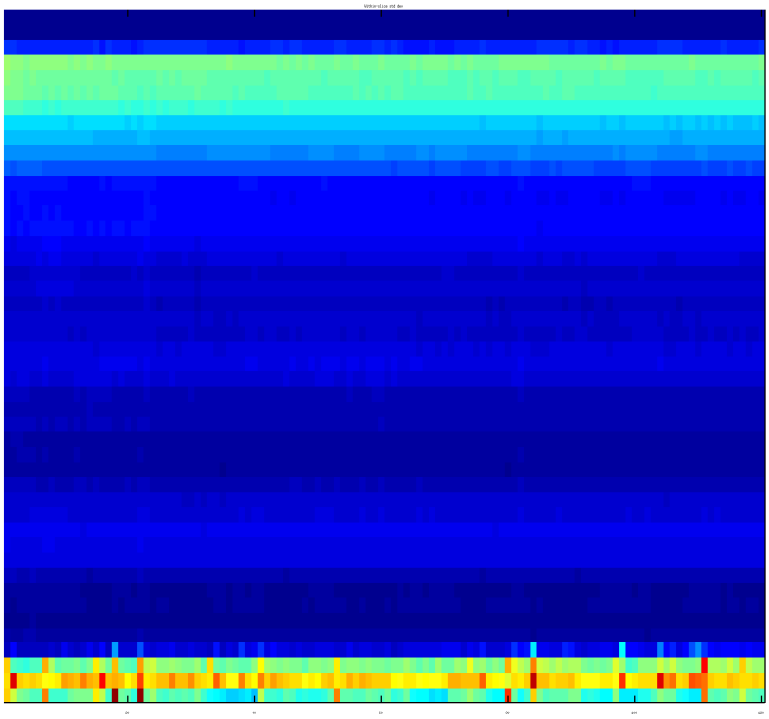

Report date: 24-Sep-2015	Matlab version: 8.1.0.604 (R2013a)

Appendix 2

Alterations of Resting State Functional Connectivity in Multiple Sclerosis at 7T

Benjamin N. Conrad, Lindsey M. Dethrage, Siddharama Pawate, and Seth A. Smith
Vanderbilt University Institute of Imaging Science (VUIIS),
Vanderbilt University, Nashville Tennessee, 37232

INTRODUCTION

- Multiple sclerosis (MS) is a disease in which the immune system attacks axons and myelin of central nervous system
- Demyelination leads to lesion formation in white matter
- Gray matter also affected but poorly understood
- Cognitive dysfunction occurs in 40-65% of MS patients [1]
- Department of Defence funded study looking at cognitive impairment in MS using multi-modal 7T brain MRI
  - Anatomical
  - Task and Resting fMRI
  - CEST and MT
  - Battery of neuropsychological tests
- Resting state fMRI (rs-fMRI) involves observation of blood-oxygen-level dependent (BOLD) signal fluctuations, which in part reflect underlying neural activity.
- Temporal correlation of the BOLD signal between voxels or brain regions serves as a measure of coactivation or functional connectivity. "*Neurons that fire together, wire together!*" [2]
- Networks detected by rs-fMRI have been shown to robustly mirror task activation patterns, providing a simple non-invasive way to assess functional brain organization. [3]
- **Objective: Perform a preliminary exploratory analysis to quantify functional connectivity differences in patients with MS compared to controls.**

MATERIALS AND METHODS

Acquisition

•Philips Achieva 7T scanner, 32-channel head coil

•Resting state BOLD scan, Single-shot EPI sequence
- 250 dynamics, scan time of 8 ½ minutes
- 2.5mm^3 isotropic voxels
- 96 x 96 x 46, slices acquired sequentially (inferior to superior)
- TR/TE/flip angle = 2s / 25ms / 63°
- Anatomical – T1wTFE , 1.25mm^3 isotropic

Preprocessing – SPM12

•Realignment to first EPI image (motion correction) [4]

•Slice timing correction

•Segmentation of T1w volume for GM, WM, CSF
- Set to "extremely light" bias regularisation and "40mm cutoff" to deal with small, irregular bias distortions at 7T

•Coregistration of skull stripped anatomical to mean functional, transform applied to tissue masks

•Normalization of coregistered gray matter mask to MNI GM template, transform applied to functional volumes

•Smoothing of functional volumes, 6mm FWHM kernel

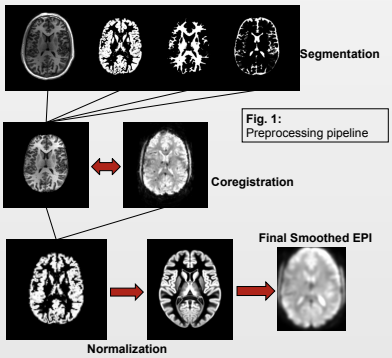

Fig. 1: Preprocessing pipeline

STATISTICAL ANALYSIS

Sample

•36 healthy controls (22 female, mean age = 30.2 ±8.5 years)

•6 MS patients (5 female, mean age = 38.8 ± 2.0 years)

1st level analysis (per subject)

•Functional voxel timeseries despiked

•Physiological noise, included as nuisance regressors
- Motion parameters
- WM and CSF signal

•Bandpass filtered 0.008-0.09hz (~ 0.5 to 5.5 cycles per minute)

Fig. 2: CONN toolbox [5]. Seed to voxel correlation map for individual subject after noise removal. Seed placed in posterior cingulate cortex.

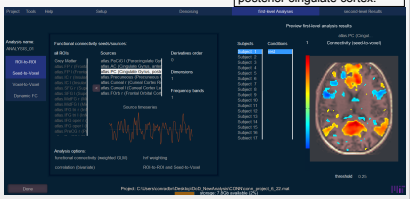

2nd level analysis (group)

•Group comparisons using Fisher-transformed correlation coefficients from source to target (regions or voxels)

•ROI to voxel connectivity
- Correlation of mean BOLD timeseries across "seed" region of interest (ROI) to all voxels

•ROI to ROI connectivity
- Correlation of mean BOLD timeseries across ROI to mean timeseries across another ROI

RESULTS

Resting state networks: Controls

•Examples of robust, large-scale rs-fMRI networks: DMN, Salience, Somatomotor, & Visual

•Finding these provides (some) assurance that the processing is working as it should

•Data below from 36 healthy controls

•Seed ROI to voxel correlation maps

•Voxel threshold at $p < 10^{-6}$, FDR and cluster corrected

Fig. 3: Default Mode Network: Associated with spontaneous thought and introspection, possibly creativity. Deactivated when focused on a stimulus or performing a cognitive task. (seed - posterior parietal cortex)

Fig. 4: Salience Network: Associated with integration and evaluation of internal stimuli, updating of one's internal state, and directing attention appropriately. Notice anticorrelation with default mode structures.[6] (seed - left frontal operculum)

Fig. 5: Somatomotor Network: Specialized cortices involved in planning, execution, and coordination of movement, including one's sense of touch and proprioception. Direct connections to cerebellum and spinal cord. (seed - right precentral gyrus/primary motor cortex)

Fig. 6: Visual Network: Tightly coupled network of occipital lobe structures, responsible for processing of information from the retina to create one's visual representation of the world, including color and motion perception. (seed - left occipital pole)

RESULTS

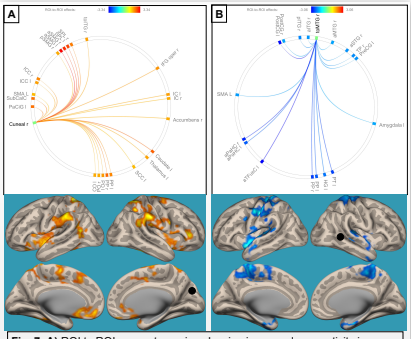

Fig. 7: A) ROI to ROI connectome ring showing increased connectivity in patients compared to controls from right cuneus. Corresponding seed to voxel map shown below (p<0.05 unc, FDR cluster p<0.05). **B)** Results showing decreased connectivity in patients compared to controls from right medial temporal gyrus (temporoccipital junction)

Functional connectivity differences in patients

•Cuneus (Brodmann Area 17)
- Basic visual processing cortex, involved in visual object recognition and spatial awareness
- Increased connectivity in patients to supramarginal gyri, multisensory integration cortices
- Finding may be related to decreased reading efficiency

•Middle temporal gyrus
- Plays role in semantic language processing (meaning) and associative memory retrieval
- Decreased connectivity to parietal and parahippocampi

DISCUSSION

- Significant alterations of regional connectivity in patients in somatosensory integration, visual, and language areas
- Increased connectivity may represent compensatory mechanisms to deal with inefficient somatosensory or visual processing
- Decreased may reflect disintegration of normal network
- Rs-fMRI may be useful in assessing neurological dysfunction on a patient-specific level, possibly before lesions appear
- Potential applications in treatment monitoring, targeted cognitive therapies or transcranial magnetic stimulation

Limitations and Future Directions

- Small patient sample, recruitment ongoing
- Presence of lesions near or within gray matter may be a confound when comparing signals of patients to controls
- Relationship of rs-fMRI to task fMRI activity
- Correlate with neuropsych measures, CEST and MT

ACKNOWLEDGEMENTS

Research supported by the following:

W81XWH-13-1-0073 (DOD/MSRP), Seth A. Smith

Vanderbilt University Institute of Imaging Science

REFERENCES

[1] Jongen et al, Minerva Med 103(2), 2012 [2] Hebb D. *The Organization of Behaviour*, 1949.

[3] Biswal. et al, MRM (34), 1995. [4] SPM12, UCL, Wellcome Trust Centre for Neuroimaging

[5] CONN Toolbox, The Gabrieli Lab. McGovern Institute for Brain Research

[6] Palaniyappan et al, J Psychiatry Neurosci 37(1), 2012.

Vanderbilt University Institute of Imaging Science

VUIIS Building, Medical Center North
1161 21st Ave. South
Nashville, TN 37232-2310

Tel: (615) 322-8359
Fax: (615) 322-0734
URL: www.vuiis.vanderbilt.edu

Appendix 3

- Network of Cuneus–SMG–Paracingulate(Prefrontal) thought to be important for visual processing of symbols/words and in reading
- May be target network given dysfunction in visual processing/visual memory commonly seen in multiple sclerosis
- Increased Connectivity from Bilateral Supramarginal Gyri (SMG) in 6 patients vs 36 controls
  Using combined average signal timecourse from right and left SMG
- Increased connectivity of this network at rest in patients may represent a compensatory effect whereby the patient brain maintains a heightened state of connectivity to overcome impairment, in a sense it remains overly primed for impending input. Alternatively the increase may be understood as a consequence of inefficient processing (overactivity) experienced in this network during normal activity.

ROI x ROI connectivity
13 significant out of out of 103 possible target regions (p<0.05 unc)

Significant Targets	beta	T(40)	p-unc	p-FDR
1. atlas.Cuneal r (Cuneal Cortex Right)	0.24	3.35	0.000898	0.051882
2. atlas.OP l (Occipital Pole Left)	0.18	3.30	0.001007	0.051882
3. atlas.LG r (Lingual Gyrus Right)	0.18	2.58	0.006768	0.232379
4. atlas.Cuneal l (Cuneal Cortex Left)	0.17	2.29	0.013793	0.233311
5. atlas.ICC r (Intracalcarine Cor*ght)	0.16	2.27	0.014464	0.233311
6. atlas.OP r (Occipital Pole Right)	0.14	2.25	0.014998	0.233311
7. atlas.PaCiG l (Paracingulate Gy*eft)	0.17	2.23	0.015856	0.233311
8. atlas.LG l (Lingual Gyrus Left)	0.16	2.10	0.021015	0.270568
9. atlas.aMTG r (Middle Temporal G*ght)	0.16	1.99	0.026662	0.305128
10. atlas.SCC r (Supracalcarine Cor*ght)	0.15	1.92	0.030814	0.317389
11. atlas.pSTG l (Superior Temporal*eft)	0.10	1.87	0.034429	0.322381
12. atlas.OFusG r (Occipital Fusifo*ght)	0.11	1.76	0.042940	0.352193
13. atlas.PaCiG r (Paracingulate Gy*ght)	0.14	1.69	0.049477	0.352193
14.				

ROI-ROI map

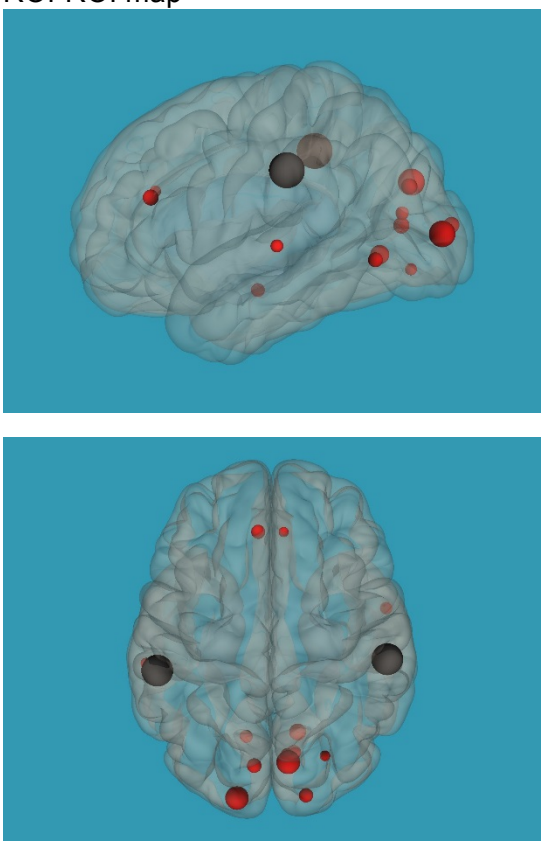

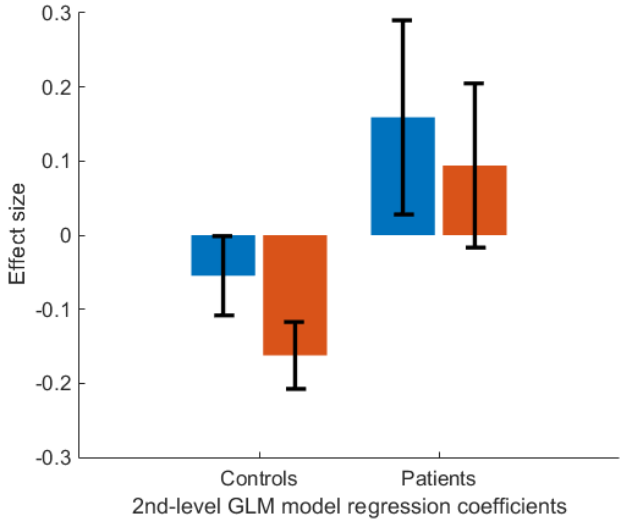

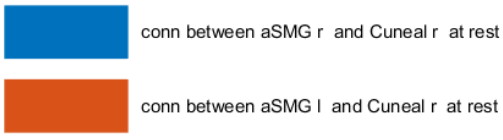

Seed-Voxel map of same analysis above

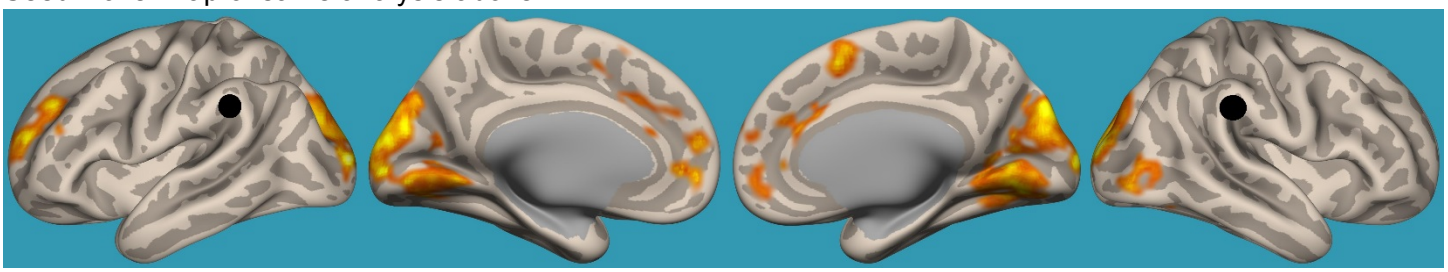

Bilateral SMG Connectivity related to Trail Making Task (TMT) in 6 patients:

- Faster TMT associated with increased connectivity of SMG to prefrontal areas ($p<0.05$, unc)
- May suggest that for the network described above, increased integration of the prefrontal component leads to faster visual processing in patients